

The fingerprints of flexure in slab seismicity

D. Sandiford^{1,2,3}, L.M Moresi^{2,4}, M. Sandiford², R. Farrington², T. Yang⁵

¹Institute of Marine and Antarctic Studies, University of Tasmania

²School of Earth Sciences, University of Melbourne

³Helmholtz Centre Potsdam - German Research Centre for Geosciences (GFZ)

⁴Australian National University

⁵Southern University of Science and Technology

Key Points:

- Intermediate depth seismicity is controlled by bending in a wide range of settings
- Geometric differences lead to contrasting seismic expression between east and west Pacific slabs
- Double seismic zones associated with bending are often masked by the strong temperature controls on seismicity

Corresponding author: Dan Sandiford, dan.sandiford@utas.edu.au

14 **Abstract**

15 Earthquake moment tensors in east Pacific (ePac) slabs typically show downdip ten-
 16 sional axes (DT), whereas in the west Pacific (wPac) they typically show downdip com-
 17 pressional axes (DC) or have mixed orientations indicative of unbending. Prevailing con-
 18 ceptual models emphasise uniform stress/deformation modes, i.e. bulk stretching or short-
 19 ening, as the dominant control on intermediate depth seismic expression. In contrast we
 20 propose that much of the diversity in seismic expression is consistent with expectations
 21 of flexural strain accumulation due to systemic differences in slab geometry. Our anal-
 22 ysis reveals two largely unrecognised features of ePac intraslab seismicity. Firstly, earth-
 23 quake clusters consistent with slab unbending are present in ePac slabs, albeit at much
 24 shallower depths than typical of wPac slabs. Secondly, intermediate depth ePac DT seis-
 25 micity is strongly localised to the upper half of zones undergoing curvature increase, such
 26 as flat slab segments. Our study highlights how the seismic expression of slab flexure is
 27 impacted by the relative contribution of brittle and ductile deformation. The strongly
 28 asymmetric temperature structure that is preserved in sinking slabs means that seismic-
 29 ity disproportionately records the deformation regime in the colder part of the slab, above
 30 the neutral plane of bending. The expression of in-plane stress may be discernible in terms
 31 of a systematic modifying effect on the seismic expression of flexure.

32 **1 Introduction**

33 Inclined zones of earthquakes extending to depths of up to 700 kms beneath vol-
 34 canic arcs delineate the geometry of subducting slabs and provide a unique insight into
 35 plate tectonics and mantle convection (e.g. McKenzie, 1969; Elsasser, 1969). To the ex-
 36 tent that rupture mechanisms of these subduction related earthquakes are thought to
 37 reflect the force balance in subducting slabs, they have been used to provide key insights
 38 into the basic mechanisms of plate tectonics. The force system in slabs includes buoy-
 39 ancy forces due to thermal and metamorphic density contrasts, flexural stress associated
 40 with slab bending and unbending, and resistance arising from slip along the subduction
 41 interface and deeper mantle penetration (e.g. Isacks & Molnar, 1971; Sleep, 1979; Fu-
 42 jita & Kanamori, 1981; House & Jacob, 1982).

43 Intermediate-depth earthquakes have traditionally been defined as those in the ~
 44 70-300 km depth range, where the subducting slab is mainly detached from the over-riding

45 plate (Gutenberg & Richter, 1954). The classic studies of Isacks and Molnar (1969, 1971)
 46 showed that either the least or most extensive moment tensor eigenvectors tends to be
 47 aligned in the slab downdip direction, consistent with the slab acting as a stress guide
 48 in a weaker mantle (Fig. 1d,h. Elsasser, 1969). They also identified that the co-seismic
 49 deformation patterns at intermediate depths correlate with broader seismic distribution
 50 in the slab. Slabs segments with no deep earthquakes, or significant gaps between inter-
 51 mediate and deep earthquakes, usually exhibit downdip tension/stretching referenced
 52 herein as ‘DT’ (Fig. 1h). In contrast, slabs with deep and continuous seismicity tend to
 53 be dominated by downdip compression/shortening, referenced as ‘DC’ (Fig. 1d). Based
 54 on these spatial relationships, Isacks and Molnar (1971) helped to establish the prevail-
 55 ing paradigm that slab earthquake orientations mainly reflect a uniaxial, or uniform, de-
 56 formation mode in the slab reference frame. The enduring nature of these insights is ex-
 57 emplified in a quote from a recent study “*slabs seem to be stretching as gravity acting*
 58 *on excess mass in the slabs pulls them down, like dangling springs hanging from and at-*
 59 *tached to lithosphere above”* (Molnar & Bendick, 2019).

60 The correlations identified by Isacks and Molnar (1971), which relate to the seis-
 61 micity patterns in individual slab segments, also expose contrasts between eastern Pa-
 62 cific slabs (ePac) and western Pacific slabs (wPac). In ePac slabs such as Chile, inter-
 63 mediate depth focal mechanisms are strongly dominated by DT earthquakes whereas wPac
 64 slabs such as Tonga tend to be dominated by DC events. DT regimes are often attributed
 65 to uniform stretching due to slab pull (Isacks & Molnar, 1971; Rietbrock & Waldhauser,
 66 2004; Bloch et al., 2018; Bailey et al., 2009), while DC regimes have been attributed to
 67 the propagation of compressional stress along the slab from interactions between the deep
 68 parts of the slab and the transition zone (Figs 1d & 1h, Fujita & Kanamori, 1981; Gur-
 69 nis et al., 2000; Billen et al., 2003).

70 In detail, it has long been recognised that slab seismicity patterns are more com-
 71 plex than either strictly DC or DT, leading to the proposition that other deformation
 72 modes such as flexure are expressed in some slabs, e.g. northern Japan, Kuriles, Tonga,
 73 northern Marianas and eastern Aleutians. In these cases, intermediate depth focal mech-
 74 anisms exhibit a systematic polarity switch, suggesting that while the upper part of the
 75 slab is in downdip compression the lower part is in down dip tension (Engdahl & Scholz,
 76 1977; Hasegawa et al., 1978; Sleep, 1979; Tsukahara, 1980; Samowitz & Forsyth, 1981;

77 Kawakatsu, 1986b, 1986a; Wang, 2002; Kita et al., 2010). Such Double Seismic Zones
 78 (DSZ) are consistent with unbending in the presence of dehydration embrittlement.

79 However, because some DSZs continue beyond the expected depths of unbending,
 80 and others have an opposite polarity to that expected from slab unbending (Comte et
 81 al., 1999), additional sources of stress have been argued to play a significant role in lo-
 82 calising DSZ seismicity (Fujita & Kanamori, 1981; Brudzinski et al., 2007). Some stud-
 83 ies have focused on DSZs as an expression of metamorphic/dehydration phenomena, of-
 84 ten without explicit consideration of the associated rupture mechanisms or sources of
 85 deviatoric stress (e.g. Peacock, 2001). Indeed, metamorphic and fluid processes have long
 86 been seen as key to intermediate depth earthquake nucleation (e.g. Isacks & Molnar, 1971)
 87 and have dominated discussions of slab seismicity in recent decades (Green & Houston,
 88 1995; Hacker et al., 2003; Kirby et al., 2013; Seno & Yamanaka, 2013; Peacock, 2001; Tsu-
 89 jimori et al., 2006; Faccenda, 2014; M. Chen et al., 2019).

90 Even allowing for the strong weakening role played by dehydration, the concept that
 91 some slabs undergo appreciable rates of stretching (10^{-15} s^{-1} , e.g. Kawakatsu, 1986a)
 92 implies high deviatoric stresses. This is because uniform stretching involves not only the
 93 deformation of a shallow, brittle part of the slab but also the deeper, ductile slab core
 94 (e.g. Capitanio et al., 2009). Conrad and Lithgow-Bertelloni (2004) argued that in or-
 95 der to produce bulk stretching rates in the order of 10^{-15} s^{-1} the effective tensional stress
 96 magnitudes may be as much as 500 MPa, assuming effective slab viscosity several hun-
 97 dred times higher than typical upper mantle. While uncertainties in slab rheology mean
 98 such stress estimates are speculative, they are not implausible given the thermal and com-
 99 positional buoyancy forces in subducting slabs are of order 10^{13} N.m^{-1} .

100 In this study we argue that strain accompanying geometric bending (Fig. 1a,e) pro-
 101 vides an important control on the seismic moment release in many Pacific margin slab
 102 settings, albeit in ways that are subtly obscured by the rheological transition from brit-
 103 tle to ductile deformation. We show, firstly, that earthquakes due to slab unbending are
 104 much more widespread than previously recognised, occurring in both ePac as well as wPac
 105 slabs. An important difference is that in ePac slabs the unbending takes place at much
 106 shallower depths than in wPac slabs. Hence, most ePac unbending earthquakes have strong
 107 spatial overlap with the megathrust zone and so have been largely overlooked in previ-

108 ous analyses. In Section 2 we describe a procedure to filter megathrust earthquakes from
109 global catalogs, that helps reveal the characteristic ePac shallow unbending signature.

110 We also show that ePac intermediate depth seismicity is conspicuously clustered
111 in the upper parts of curvature-increasing zones associated with full or partial slab flat-
112 tening. In such zones, we speculate that seismicity is mainly restricted to the cold, up-
113 per half of the slabs, where they evidence down-dip stretching and that the associated
114 shortening in the lower half of the slab is largely accommodated aseismically. Crucially,
115 while the larger earthquakes reported in the global catalogs tend to show uniform inter-
116 mediate depth DT seismicity, microseismic studies in Chile have revealed oppositely-polarised
117 DSZs (Comte & Suarez, 1994), consistent with flexure. For geometric bending to be ex-
118 pressed so prominently, strain rates associated with flexure (Fig. 1b,f) must be compa-
119 rable to, or exceed, those associated with uniform stretching modes due to, for exam-
120 ple, slab pull (Fig. 1d,h). This is consistent with the notion that slab buoyancy is largely
121 supported by drag in the upper mantle. Variations in the uncompensated slab pull com-
122 ponent will impact the relative location of the bending neutral plane with respect to the
123 brittle ductile transition. This effect can have a strong impact on seismic expression, var-
124 iously enhancing or impeding seismicity beneath the neutral plane.

125 **2 Terminology, methods and manuscript structure**

126 In seismology the term ‘intermediate-depth’ typically refers to subduction related
127 earthquakes with hypocentral depths in the range 70-300 km. We argue that the restric-
128 tion to events deeper than about 70 kms has imposed somewhat arbitrary limitations
129 on analyses of subduction related seismicity. Here we use the term ‘slab’ or ‘intraslab’
130 earthquakes to refer to all earthquakes within the subducting lithosphere from the on-
131 set of bending near the outer-rise to the deepest limit of seismicity at ~ 700 km. How-
132 ever, our analysis focuses only on earthquakes shallower than 300 km. This is because
133 uncertainties in slab geometry as well as earthquake hypocenters increase with depth.
134 In addition, slab earthquake activity rates are typically very low at depths of around 300
135 km (e.g. Vassiliou et al., 1984). As a consequence, our methods are not well suited to
136 depths beyond a few hundred kilometres. Importantly, we assume no intrinsic distinc-
137 tion between earthquakes with hypocentral depths above and below 70 km. We still oc-
138 casionally refer to the intermediate depth range, as this remains a familiar specification
139 of a particular depth range.

140 We also consider the term ‘outer-rise’ earthquakes is something of a misnomer be-
141 cause earthquakes that result from the bending of the incoming plate are concentrated
142 in the outer trench slope and often extend landward of the trench to regions of the slab
143 beneath the shallow part of the fore-arc.

144 Hence we will refer to the region where the incoming plate experiences increasing
145 curvature as the ‘outer bending zone’ (or OBZ). Downdip of the OBZ, after passing through
146 peak curvature, slabs invariably straighten in a zone of unbending which we term the
147 primary unbending zone (or PUZ). These regions are labelled in Fig. 1a.

148 In discussing contributions to the slab deformation rate, we emphasise the distinc-
149 tion between flexural and uniform modes (see Fig. 1). We use the terms flexure and bend-
150 ing somewhat interchangeably, in keeping with historical developments in the literature.
151 Flexural strain is associated with changes in curvature. Curvature is considered positive
152 when the slab curvature is concave down. Material may respond to a change in curva-
153 ture in a number of ways, for instance by simple bending, or by flexural slip. While flex-
154 ural slip has been discussed in relation to slab seismicity (Romeo & Álvarez-Gómez, 2018),
155 our study focuses on simple bending, in which cross-sections orthogonal to the plate re-
156 main planar. In this case the total strain is proportional to the curvature, and is char-
157 acterised by anti-symmetry across the neutral plane. Regions where curvature is increas-
158 ing, for example, are associated with downdip extension above and compression below
159 the neutral plane. Arguments that bending/unbending is a controlling factor stem pri-
160 marily from the observation polarity switches in earthquake moment tensors in double
161 seismic zones (DSZ). In contrast, for a ‘uniform’ mode of slab deformation, involving ei-
162 ther bulk slab stretching or shortening in the downdip direction, such polarity switches
163 are precluded.

164 Strain rates associated with changes in curvature can be separated into a time de-
165 pendent and advective component. Where the morphology of the slab is changing in time,
166 for instance a reduction in the curvature radius associated with slab steepening, there
167 is a time dependent component of the curvature rate. However, even if the morphology
168 is stationary, bending still occurs where material passes through finite curvature gradi-
169 ents. This component of the curvature rate is often referred to as advective (Ribe, 2010;
170 Buffett & Becker, 2012) or kinematic (e.g. Kawakatsu, 1986a). Here we use the term ‘ge-

171 ometric bending’ to emphasise the association between the bending rate and the downdip
172 curvature gradient.

173 It is important to note that bending is a description of strain, and implies no spe-
174 cific constitutive behavior. In particular, the reader should be wary of thinking in terms
175 of elastic sheet mechanics. If slabs behaved as perfectly elastic sheets stress would vary
176 systematically with the total curvature e.g. Fig. 1c,g), and in the process of unbending
177 the plate would simply return to an undisturbed elastic state. The occurrence of inter-
178 mediate depth seismicity, along with a range of other observations, provides a strong ar-
179 gument that this is not the case (Chapple & Forsyth, 1979; Goetze & Evans, 1979; Billen
180 et al., 2003; Sleep, 2012).

181 In describing the relationships between between slab geometry and seismicity, we
182 refer frequently to the slab midplane. We use this term in relation to both observed slab
183 geometries (sections 3 and 5) and the analysis of a numerical model (section 4). The no-
184 tion of a midplane serves as a proxy for the neutral plane of bending, which plays a key
185 role in determining the way deformation responds to changes in curvature. The estima-
186 tion and applicability of the midplane is discussed in more detail in the supplementary
187 material.

188 The term ‘seismic expression’ refers to the spatial distribution of hypocenters along
189 with the associated moment tensors. Slab dynamics in idealised flexural and uniform modes
190 is very different (Fig 1, and we would expect the seismic expression to reflect this to some
191 degree. In addition to the dynamic state of the slab, the seismic expression is obviously
192 very dependant on the relative contribution of brittle and ductile deformation.

193 Our analysis primarily focuses on relationships between earthquake data and slab
194 geometry, and so is limited by uncertainties in both. A detailed outline of our methods
195 are provided in the supplementary material, which covers our treatment of earthquake
196 data, and numerical methods. We combine the global CMT (Ekström et al., 2012) and
197 EHB (Engdahl et al., 1998) catalogs, to improve depth uncertainties and relate them us-
198 ing the either the Slab1 (Hayes et al., 2012) or Slab2 (Hayes et al., 2018) models, as dis-
199 cussed in the supplementary material. A novel step is our filtering of shallow intraslab
200 earthquakes from those on the subduction interface, as briefly described below.

201 ‘Megathrust’ earthquakes on the subduction interface constitute a very significant
 202 proportion of the overall seismic activity in the shallow part of subduction zones. Al-
 203 though megathrust seismicity does not overlap spatially with intermediate depth earth-
 204 quakes *sensu stricto* (> 70 km), filtering of potential megathrust events is extremely im-
 205 portant in terms of identifying intraslab seismicity at shallow depths beneath the fore-
 206 arc wedge. Even with well resolved depth locations, uncertainties mean we cannot un-
 207 ambiguously discriminate intraslab from megathrust events on hypocenter data alone.
 208 The filtering procedure we use defines the strike and rake of the reference megathrust
 209 rupture tensor (\mathbf{M}^{ref}), assuming a pure double-couple mechanism. A similarity condi-
 210 tion (χ) for a given earthquake with (\mathbf{M}^k) is referenced to the tensor dot product ($:$) of
 211 the normalised moment tensors:

$$\chi = \left[\frac{\mathbf{M}_{ij}^{\text{ref}} : \mathbf{M}_{ij}^k}{|\mathbf{M}^{\text{ref}}| |\mathbf{M}^k|} \right] \quad (1)$$

212 We assume an event is a megathrust rupture if it has a hypocentral depth less than
 213 70 km and is within 20 km of the relevant slab surface model and a similarity condition
 214 of $\chi \geq 0.75$. Further details are provided in the supplementary material.

215 The manuscript is structured as follows. Section 3 provides a summary of the seis-
 216 mic expression and morphology of representative Pacific margin slab sections, highlight-
 217 ing key features that motivate our analysis. Section 4 summarises insights of slab dy-
 218 namics drawn from a numerical subduction model in which flexural modes dominate the
 219 strain rate field. Drawing on the modeling insights, Section 5 revisits the observations
 220 presented in section 3 to examine the specific relation between seismicity and curvature
 221 gradients needed to assess the role played by geometric bending. In the Discussion we
 222 summarise the main findings, and explore some of the broader issues that stem from them.

223 **3 Comparative seismology and geometry of the Pacific slabs**

224 In this section we compare three wPac slab segments (Fig. 2) in Tonga, Japan, and
 225 the Kuriles, and three ePac slab segments (Fig. 4) in Chile, Peru and Central America,
 226 using trench perpendicular transects to provide a regional overview of both slab geom-
 227 etry and seismicity. While deep (> 300 km) seismicity is portrayed in some of the ac-
 228 companying figures, our analysis is restricted to earthquakes shallower than 300 km. In
 229 our representations (e.g. Fig. 2a), coloured points show earthquakes designated as in-

230 traslab events, while earthquakes that lie more than 20 km above the projected slab sur-
 231 face, in the slab normal direction, are shown as small black points. Because the along-
 232 strike slab morphology tends to more variability with depth, the deviation in hypocen-
 233 ters from a ‘region-average’ slab geometry increases with depth. This accounts, for in-
 234 stance, for the large number of outliers in Tonga at depths > 300 km. However, the ‘region-
 235 average’ slab geometries generally provide a consistent fit to slab seismicity at depths
 236 less than 300 km for most of the regions described here. There are some complexities
 237 in the case of the ePac slabs, discussed in more detail later.

238 We represent the orientation of slab earthquake moment tensors by projecting the
 239 T-axis onto trench-perpendicular vertical sections (e.g. Fig. 3). The T-axes projections
 240 are not scaled by magnitude, so their projected length reflects the difference in azimuth
 241 of moment tensor eigenvectors with respect to the trench normal direction. We note T-
 242 axes necessarily lie within the quadrant with the smallest stress eigenvector and are com-
 243 monly assumed to represent the orientation of most extensive co-seismic strain release
 244 (Isacks & Molnar, 1971; Bailey et al., 2009; Yang et al., 2017). The color of the T-axes
 245 represents the angle relative to the local slab orientation. Red colours are DC events,
 246 blue are DT events.

247 Seismicity associated with the OBZ is clearly evident in each of the wPac regions,
 248 with the onset of characteristic normal faulting events distances of around 50 km sea-
 249 ward of the trench in Tonga and 100 km in Japan and the Kuriles. In all cases this DT
 250 seismicity appears to continue, in a largely continuous manner, landward of the trench,
 251 up to about 70 km in the case of Tonga. As discussed later, this suggests that the cur-
 252 vature of the slab continues to increase downdip from the trench. This morphological
 253 property is corroborated in the Slab1 model, which represents a surface fit to the seis-
 254 micity (discussed in more detail in section 5). Yet, it runs counter to typical models of
 255 elastic or elastic-plastic plate flexure (Caldwell et al., 1976), where unbending occurs be-
 256 fore the trench, even when the influence of yielding is carefully considered (Chapple &
 257 Forsyth, 1979). Deeper DC events in the OBZ are generally viewed having a reciprocal
 258 flexural origin to DT ones, reflecting shortening beneath the neutral plane (Chapple &
 259 Forsyth, 1979; Craig et al., 2014). Based on the datasets used in this study, only Tonga
 260 exhibits an unambiguous record of deep DC events in the OBZ. The onset of these events
 261 is virtually coincident with the shallower DT events, at around 50 km from the trench.
 262 In the Kuriles and Japan the number of potential DC events is very low compared with

263 the OBZ normal faulting events. Nevertheless, DC OBZ events are documented in both
 264 regions (Craig et al., 2014), as evidenced by a recent (2020-03-25) Mw 7.5 earthquake,
 265 with a hypocenter at 55 km depth located almost directly under the Kuriles trench (depth
 266 based on USGS finite fault model).

267 Historically, the role of unbending in slab seismicity has mainly been discussed in
 268 relation to the Kuriles, Japan, Tonga, Aleutians, and northern Marianas (Engdahl & Scholz,
 269 1977; Hasegawa et al., 1978; Kawakatsu, 1986b, 1986a; Tsukahara, 1980; Samowitz &
 270 Forsyth, 1981; Wang, 2002). The key feature of these regions is the DSZs with a char-
 271 acteristic ‘polarity’ switch in moment tensor between an upper band dominated by DC
 272 events and a lower band dominated by DT events. This distribution is very clear in the
 273 Kuriles slab (Fig. 3b) where a clear offset in the locus of DC and DT events occurs at
 274 depths between 70 - 200 km. The polarity switch is also evident in both Tonga and Japan,
 275 although in both cases the relative proportion of lower plane DT to upper plane DC events
 276 is lower than in the Kuriles (e.g. Kawakatsu, 1986b). Importantly, while the PUZ in both
 277 Tonga and Japan is dominated by DC events, neither are exclusively DC (Figs. 3a,b),
 278 and in both instances DT events are systematically deeper. As we discuss further be-
 279 low this is contrary to the expectation of uniform slab shortening proposed in previous
 280 studies (e.g. Isacks & Molnar, 1971; Richter, 1979; Fujita & Kanamori, 1981).

281 In Japan a polarised DSZ is clearly evident in the PUZ at depths between 60 and
 282 200 km. Compared with the Kuriles, lower plane DT events are more clustered, and oc-
 283 cur further downdip than the upper plane DC counterparts. The great Tohoku megath-
 284 rust event in 2011 occurred during the catalog interval considered here, resulting in a
 285 large cluster of extensional earthquakes in the shallow part of forearc (labelled in Fig.
 286 3c, Imanishi et al., 2012). The Tohoku earthquake also intraslab earthquake rates. For
 287 example, a comparison of Figs. 3c&d suggests that OBZ activity rates following the To-
 288 hoku earthquake have been substantially elevated, consistent with a positive static stress
 289 change. Interestingly, the number of unbending (PUZ) events did not increase to the same
 290 extent. In particular very few additional lower plate (DT) events occurred since 2011.
 291 This suggests that stress changes following to the megathrust rupture were less signif-
 292 icant in the deeper part of the slab than in the shallower incoming parts. These obser-
 293 vations reinforce the notion that even when geometric bending strain accumulation is
 294 expected its seismic expression is quite variable, and can be impacted over timescales

295 of at least a decade by associated large megathrust ruptures. Despite the changes in seis-
 296 micity rates since 2011, the seismic expression appears similar to earlier events.

297 The along-strike morphology of ePac slabs tends to be more variable than wPac
 298 slabs and includes prominent flat slab segments in Chile (Pampean), Peru and Mexico.
 299 An important consequence is that ePac slabs commonly exhibit additional zones of bend-
 300 ing and unbending downdip from the PUZ. An issue in characterising ePac seismicity
 301 relates to the relatively low rates of OBZ and PUZ seismicity. Resolving their seismic
 302 expression requires aggregating earthquakes over significant distances along strike (~ 1000
 303 km). Because the slab morphology is relatively coherent at shallow depths, the analy-
 304 sis of aggregated earthquakes in the OBZ and PUZ is typically quite straightforward.
 305 However, with increasing downdip distance this coherence degrades and the deeper slab
 306 seismic expression of ePac slabs tends to be less well resolved compared to wPac slabs.
 307 These issues are most significant in Chile in the vicinity of the Pampean flat slab where
 308 the Juan Fernandez ridge subducts beneath the Andes (Fig. 4a). However, here we treat
 309 the entire region as a single extended domain because: a) the Pampean flat slab is rel-
 310 atively narrow and has low intermediate depth seismicity rates compared to the north-
 311 ern part of the Chile slab (i.e. the north Chile seismic belt, shown in Fig. 4a) and b) OBZ
 312 and PUZ seismicity rates are generally low but much more uniformly distributed, and
 313 so the extended domain provides a well resolved view of OBZ and PUZ seismicity.

314 Compared with wPac settings, ePac OBZ seismicity tends to be clustered much closer
 315 to the trench and with much fewer events. In Peru, OBZ events are located within about
 316 10 kms, with a locus of activity slightly landward, of the trench (Fig. 5a). In the PUZ,
 317 clusters of earthquakes occur about 100 km inboard of the trench in Chile, and 150 km
 318 in Peru (Figs. 5a&b). In both cases a band of dominantly DC events overlies a smaller
 319 band of DT events. As discussed in Section 5, these events occur in regions where in-
 320 ferred rates of PUZ unbending are highest. The relatively shallow depths of ePac PUZ
 321 seismicity means it partly underlies the megathrust zone, and so filtering megathrust events
 322 is critical to their resolution. While the significance of ePac DC events in terms of a pu-
 323 tative unbending DSZ was noted as long ago as 1976 (e.g. Barazangi & Isacks, 1976) it
 324 has largely been overlooked, and other studies have argued for alternative explanations
 325 such as slab-push (Lemoine et al., 2002) and flexural slip (Romeo & Álvarez-Gómez, 2018).

326 Downdip from the PUZ, the morphology of the Chile and Peru slabs deviates sub-
 327 stantially. Peru has a very long (~ 300 km) flat slab region, followed by a second zone
 328 of steepening along the distal hinge of the flat slab section. The peak in curvature oc-
 329 curs at around 600 km from the trench. The ‘regional-average’ slab morphology for Chile
 330 (Fig. 5a) does not contain a prominent flat slab *sensu stricto*. However, a subtle upwards
 331 deflection beginning at around 200 km from the trench is indicative of partial flatten-
 332 ing. Despite its subtle form, the implied curvature gradient is significant, consistent with
 333 high flexural strain rates.

334 In both Chile and Peru, slab seismicity at classic ‘intermediate depths’ is dominated
 335 by DT events. In Peru, DT seismicity is distributed throughout the flat slab, becoming
 336 more frequent towards the distal hinge, with an average depth of ~ 120 km and a slight
 337 concave up distribution when projected on slab normal sections (see supplementary Fig.
 338 S6). A cluster of earthquakes known as the Pucallpa seismic nest (Fig. 5c) is located prox-
 339 imal to a localised depression in the slab along the distal hinge of flat slab (Gutscher et
 340 al., 2000; Wagner & Okal, 2019). In Chile, the DT events are clustered in two zones. The
 341 first overlaps with the zone of partial slab flattening, between 200 and 350 kms from the
 342 trench, centered at a depth of ~ 110 km (as depicted by red points in Fig. 4a). The sec-
 343 ond cluster is more diffuse, concentrated between 400 and 500 km from the trench and
 344 depths of 150-300 km (displaying as blue points in Fig. 4a). As most evident in trench-
 345 parallel section (see Supplementary Fig. S6) the shallower zone forms a sub-horizontal
 346 band best developed in the north (labelled ‘north Chile seismic belt’) but clearly present
 347 in parts of the slab further south. The deeper second zone forms a steeply oriented band
 348 shallowing to the south (highlighted with a red dashed line in Fig. S6) The clustering
 349 of these earthquakes is indicative of deformation with strong lateral variability. Our study,
 350 which focuses on flexural deformation in the 2d trench perpendicular plane, is unable
 351 to determine any meaningful geometric correlations when such clear along-stroke (or 3d)
 352 variations are present.

353 The projections onto the ‘regional average’ slab model highlight the anomalous na-
 354 ture of the slab models for Peru. For all other slabs, the locus of intermediate depth seis-
 355 micity occurs in the upper 20-30 kms of slab, at or above the slab midplane, consistent
 356 with the expectation that seismicity is concentrated in the cooler parts of the slab (Emmerson
 357 & McKenzie, 2007). For Peru, intermediate depth seismicity projects at a significantly
 358 deeper level relative to the slab models, mostly below the midplane. We suspect this re-

359 flects systemic errors in the slab models for Peru, as for example identified by Rosenbaum
360 et al. (2019), with the Slab2 model around 20-30 kms too shallow.

361 The Central American slab is the most seismically incoherent of the slabs sections
362 described here, presumably because morphological variability blurs the patterns of ag-
363 gregated seismicity, even at shallow depths (Fig. 5c). Hypocenter locations exhibit sub-
364 stantial scatter at all depths, and less pronounced downdip clustering evident in both
365 Chile or Peru. Based on the region-averaged geometry, the Central America slab is char-
366 acterised by two distinct zones of steepening (Fig. 5c). After bending through the OBZ,
367 the slab unbends fully at about 100 km distance from the trench, before steepening again
368 with a second peak in curvature at about 175 km. Unlike the other ePac slabs, there is
369 no distinct reduction in dip angle between the peaks in positive curvature (we note that
370 a little further north beneath Mexico there is a prominent flat slab, which shows many
371 similarities to the Peruvian flat slab in terms of relationships between seismicity and ge-
372 ometry as discussed in detail by D. Sandiford et al. (2019)). The majority of earthquakes
373 in this segment of the Central American slab have DT mechanisms and are concentrated
374 at a distance of about 130 km from the trench in a zone of curvature increase where, sim-
375 ilar to the outer rise, flexural stretching of the upper part of the slab is expected. While
376 several DC events (red axes in Fig. 5c) could potentially indicate unbending in the PUZ,
377 there is no clear spatial separation between DC events and the more numerous DT earth-
378 quakes. Moreover, Fig. 5c shows that the principal axes of the DC events are not pref-
379 erentially aligned with the slab dip direction, as is expected for flexural unbending, and
380 may reflect a more prominent role for out of plane bending or that the variations in slab
381 morphology are significant and poorly represented by the region-average geometry.

382 **4 Insights from numerical modeling**

383 In this section we describe results of a numerical subduction model, which provides
384 insight into the relative contribution of different modes of slab deformation, as well as
385 the geometric controls on flexural deformation. The setup is comparable to recent stud-
386 ies, where flow is driven entirely by the thermal density contrast of the plate-slab, which
387 develops as a naturally evolving thermal boundary layer at the surface (Garel et al., 2014;
388 Agrusta et al., 2017). The model setup is described in detail in the Supplementary ma-
389 terial (see also D. Sandiford & Moresi, 2019). Mantle rheology (including oceanic litho-
390 sphere) is prescribed by a composite flow law including linear high-temperature creep

391 and a scalar visco-plasticity designed to capture both psuedo-brittle as well as distributed
 392 plastic deformation within the slab. We assume the stored elastic stress component is
 393 relaxed over relatively short time/length scales and can be neglected.

394 An important feature of the model is the evolution of partial slab flattening. This
 395 morphological evolution is concomitant with a overall reduction in subduction velocity
 396 between 10 and 25 million years, and a shift to intense shortening of the upper plate. In-
 397 deed this shared set of features has been discussed in a number of recent modelling stud-
 398 ies, in terms of interplay between the sinking/retreating slab and the structure of the
 399 compensating return flow (Faccenna et al., 2017; Yang et al., 2019). In particular, the
 400 dynamics exhibited in 2d models, where the trench is capable of retreat but toroidal flow
 401 is absent, bears a close resemble to Chilean-type subduction systems, consistent with the
 402 idea that the central Andean orocline represents a stagnation point for upper mantle toroidal
 403 flow (Russo & Silver, 1994).

404 Fig. 6 shows the downdip component of the strain rate ($\dot{\epsilon}_{ss}$) at two time intervals,
 405 with the top panels in each figure showing the normalised value of curvature and cur-
 406 vature gradient evaluated along the slab midplane. The fact that flexural deformation
 407 dominates the strain rate field is evident in the strong polarisation, with zones of short-
 408 ening (red) on one side of the slab always accompanied by similarly elevated stretching
 409 (blue) on the other side. Despite the flow being driven by the thermal buoyancy contrast
 410 of the slab, the fact that the slab strain rates are polarised rather than uniform, implies
 411 that the slab pull force is substantially compensated by drag in the mantle. This sub-
 412 duction style is often referred to as the Stokes regime (Schellart, 2004; Capitanio et al.,
 413 2007; Ribe, 2010). The stress in the subducting plate at 10 myr is shown in the inset in
 414 Fig. 6. The peak stress of order 10 MPa is an order of magnitude lower would be than
 415 anticipated if a significant component of the buoyancy deficit were transmitted to the
 416 trailing surface plate (i.e. when the slab pull factor is ~ 0.5 , e.g. Conrad & Lithgow-Bertelloni,
 417 2004).

418 The model also highlights the strong geometric control on deformation rates for
 419 slabs in the Stokes regime. For a slab that deforms by pure bending, the distribution of
 420 strain rate in the downdip direction ($\dot{\epsilon}_{ss}$) is a function of the curvature rate multiplied
 421 by distance from the midplane (Tsukahara, 1980; Kawakatsu, 1986a; Ribe, 2001):

$$\dot{\epsilon}_{ss} = -y \frac{DK}{Dt} = -y \left(\frac{\partial K}{\partial t} + u_s \frac{\partial K}{\partial s} \right) \quad (2)$$

422 where s refers to a unit vector along the slab midplane, y is the distance perpendicular
 423 to the midplane, $\frac{D}{Dt}$ is the material derivative following s , K is the curvature and u_s is
 424 the velocity component parallel to the midplane. The term $u_s \frac{\partial K}{\partial s}$ is sometimes referred
 425 to as the advective or kinematic bending rate but we use the term geometric bending
 426 rate to emphasise the fact that it is the present day slab geometry that constrains the
 427 time-independent component of the bending rate.

428 Fig. 6 shows that the curvature gradient ($\frac{\partial K}{\partial s}$) correlates strongly with the downdip
 429 strain rate in the model ($\dot{\epsilon}_{ss}$), with both tending to zero as the local curvature ampli-
 430 tude maximizes as expected when geometry is a dominant control on the both the to-
 431 tal bending rate and the overall slab deformation rate. At 10 Myr, a rather typical slab
 432 morphology is characterised by plate bending outboard of the trench (OBZ) with un-
 433 bending in the PUZ centered at around 70 km depth. At 25 Myr, an upward deflection
 434 at intermediate depths produces a secondary positive curvature gradient zone charac-
 435 terised by extension in the upper part of the slab above a zone of shortening in the lower
 436 half bearing a marked similarity to the partial flattening of the Nazca slab in northern
 437 Chile (Fig. 4a).

438 Because the brittle ductile transition in lithospheric mantle is thought to occur at
 439 a potential temperature near 600 °C (Emmerson & McKenzie, 2007), the distribution
 440 of slab temperature is key to understanding the seismic expression of slab deformation.
 441 In our model, the gradual reduction in subduction velocity between 10 myr and 25 myr
 442 means the maximum depth of the 600 °C isotherm reduces from about 300 km to less
 443 than 150 km over that time interval. We note that because the modelled 600 °C isotherm
 444 encloses the upper-half of each bending region, we expect the seismic strain release would
 445 be strongly asymmetric and mainly restricted to part of the slab above neutral plane.
 446 For a given slab the degree of seismic asymmetry will likely be sensitive to its thermal
 447 structure, as well as variations in the level of in-plane stress (Craig et al., 2014).

448 5 Seismicity-geometry relationships

449 In this section we explore the relationship between geometric bending and the seis-
 450 mic expression of each of the Pacific margin slabs discussed in Section 3. Within each

451 slab region, the relative variation in the geometric bending rate is associated with downdip
 452 curvature gradient of the neutral plane, in accord with Equation 2. We calculate cur-
 453 vature gradient using the estimated slab midplane as a proxy for the neutral plane, as
 454 described in the supplementary material. To visualise these relationships we project the
 455 earthquake T-axes in a slab midplane coordinate system, with distance from the hypocen-
 456 ter to the midplane shown on the vertical axis, and distance along the midplane rela-
 457 tive to the trench on the horizontal. As in the earlier figures, the T-axes are projections
 458 on to a trench normal plane, in this case they are additionally rotated so that the an-
 459 gles relative to the midplane is preserved.

460 Figure 7 shows seismicity geometry relationships for the wPac regions. The cur-
 461 vature gradient profiles associated with wPac slabs show a relatively symmetric positive
 462 peak, with a half-wavelength of between 150 - 200 km. Peak curvature (zero gradient)
 463 occurs at a considerable distance (50 - 100 km) downdip from the trench. Beyond this,
 464 the downdip gradient changes sign and thereafter tends to decay monotonically as the
 465 slab fully straightens in the mid upper mantle.

466 In wPac slabs, OBZ earthquakes tend to cluster either near the peak in positive
 467 curvature gradient (e.g. Kuriles), or between the peak in curvature gradient and the peak
 468 in curvature (e.g. Japan, Tonga), but not at the peak in curvature. A key feature of all
 469 wPac slabs is the shift from dominant DT earthquakes to dominant DC earthquakes in
 470 the upper slab accompanying the transition from OBZ to PUZ where the curvature gra-
 471 dient switches sign. This statement neglects the shallow normal earthquakes landward
 472 of the Japan trench, as these are assumed to originate in the forearc (as labelled in Fig.
 473 7c). Nevertheless, there are some obvious differences in the seismic expression. For ex-
 474 ample, in the Kuriles the OBZ-PUZ transition is marked by a zone of relatively intense
 475 seismicity, where T-axes orientation is somewhat disorganised, before the characteris-
 476 tic polarised unbending DSZ emerges. In this transitional region many of the DC T-axes
 477 are slightly CCW rotated from the slab orthogonal/vertical. This may indicate the pres-
 478 ence of unidentified megathrust events. In Tonga, the transition in T-axis polarity is sharper,
 479 and coincides remarkably closely with the change in sign of the curvature gradient. In
 480 Japan, the transition to negative curvature gradient coincides with the onset of upper-
 481 plane DC seismicity, whereas lower plane DT events only appear a further 100 km downdip.
 482 Whereas Tonga shows a much higher proportion on upper plane DC to lower plane DT
 483 events, the Kuriles is characterised by a more symmetrical distribution.

484 The seismicity-geometry relationships for ePac slabs are shown in Fig. 8. As noted
 485 in Section 3, compared with wPac slabs, there are far fewer OBZ ePac earthquakes. Those
 486 that do occur cluster landward of the peak in curvature gradient and, as in wPac slabs,
 487 they tend to cluster between the peak in curvature gradient and the peak in curvature,
 488 rather than coinciding at peak curvature. In Peru OBZ earthquakes occur beneath the
 489 trench itself.

490 Importantly, the Peru and Chile projections highlight the key and hitherto largely
 491 overlooked point that the OBZ-PUZ transition, at the point where the curvature gra-
 492 dient switches sign, marks a switch from dominant upper plane DT earthquake to DC
 493 earthquakes, just like wPac slabs. Moreover, Figs. 8a&c shows that the ePac PUZ DC
 494 events are clustered in zones where unbending rates are highest (i.e. at maxima in the
 495 absolute curvature gradient). The key insight is that despite occurring at shallower depths
 496 than in the wPac, the distributions of PUZ earthquakes in all but the Central Ameri-
 497 can Slab are consistent with a common mechanism. The Central America is the excep-
 498 tion, with the zone of normal faulting (DT) continuing in the landward direction past
 499 the point when the curvature gradient changes sign. These patterns clearly do not fit
 500 with the systematic variation with geometric bending observed elsewhere.

501 Whereas the wPac slabs unbend monotonically, the ePac slabs typically exhibit ad-
 502 ditional zones of positive (and negative) curvature gradients. In northern Chile, a zone
 503 of positive curvature gradient occurs at about 200 km downdip from the trench (Fig. 8a),
 504 corresponding to the partially flattened slab, which is expected to induce flexural exten-
 505 sion in upper half of the slab. This zone has a strong spatial overlap with the belt of DT
 506 seismicity along the Chile slab at ~ 100 km depth, the most active expression being the
 507 north Chile seismic belt (see Fig. 4a and supplementary Fig. S6). The full downdip seis-
 508 mic expression is most spectacularly revealed in Chile, where a remarkable set of tran-
 509 sitions from upper plane DT (OBZ) to DC (PUZ) and then back to DT quakes is ev-
 510 ident where the slab is partially flattened. In each case the transition correlates with a
 511 change in sign of the curvature gradient, and minima in seismic activity rates.

512 There are several caveats in relating the intermediate depth earthquake belt in Chile
 513 with fluxural deformation. The first is the near-absence of deeper DC events in the CMT
 514 catalog, as would be expected by the positive bending rate. Ultimately, we argue that
 515 this is simply the result of predominately ductile deformation beneath the neutral plane.

516 These interpretation is elaborated in the Discussion section. Nevertheless, there is frag-
 517 mentary evidence in the seismic record that shortening underlying the neutral plane can
 518 lead to seismic rupture. In a regional study of micro-seismicity, Comte et al. (1999) re-
 519 solved DC events which were systematically deeper than the DT events, a pattern they
 520 referred to as an oppositely polarised DSZ. Araujo and Suárez (1994) discuss a well-located
 521 DC event at a depth of 152km, around 35 km below the cluster of DT events. They posit
 522 that this inverted DSZ may be linked to the flexural stresses induced by the change in
 523 dip. A second issue is a small number of DT events that project well below the inferred
 524 mid-plane and would seem to be more consistent with uniform downdip stretching of the
 525 slab. Given the lateral variability in Chile slab morphology, we suspect these anomalously
 526 deep DT events are mislocated when projected onto our ‘regional-average’ projection.
 527 To test this, Fig. 5d shows a section covering a narrower region within the north Chile
 528 seismic belt. For this smaller region, in which such projection uncertainties are signif-
 529 icantly reduced, a very high proportion of hypocenter locations project in the upper \sim
 530 20 km of the slab, consistent with DT seismicity being localised in a rather narrow re-
 531 gion, consistent with a restricted brittle strain regime situated above the neutral plane.

532 While the distribution of seismic activity rates across the Peru flat slab matches
 533 the general form of the curvature gradients (Fig. 8b), as noted earlier the projection places
 534 the majority of these events beneath the slab midplane of the Slab2 model. There is no
 535 record of deeper DC events in this region, and so the significance of this distribution re-
 536 mains uncertain. However, as noted the locus of Peruvian intermediate depth seismic-
 537 ity is much further below the projected slab surface than for Chile, as well as the other
 538 slabs analysed here. This suggests systematic errors in the Slab2 model for the Peruvian
 539 flat slab, with the model surface likely in error by 20-30 kms, and likely underestimat-
 540 ing the extent of flattening, which may even lead to negative dip angle at \sim 500 km from
 541 the trench.

542 In Fig. 8b a group of slightly deeper earthquakes include the Pucallpa seismic nest
 543 cluster at the distal edge of the domain at distances $>$ 650 km from the trench, in a re-
 544 gion of negative curvature gradient (Fig. 8b). These events are proximal to a relative
 545 localised lateral perturbation of the slab morphology, at the landward edge of the flat
 546 slab, (Gutscher et al., 2000; Wagner & Okal, 2019). This suggests that the role of out-
 547 of plane slab deformation may be significant in this region. Lateral geometric variations,
 548 or time-dependent modes of deformation (i.e. changes in slab geometry that are occur-

ring in an upper plate reference frame) can be expected to contribute to the slab strain rate field in ways the obscure down-dip gradients.

6 Discussion

In view of the many sources of uncertainty, attempting to elucidate the contribution of geometric bending from the seismic expression of deforming slabs represents a significant challenge. As discussed earlier, the sources of uncertainty include the earthquake hypocenters, slab geometry models, the impact of out of plane bending and other modes of deformation, and finally the confounding effects of temperature and metamorphism in promoting or impeding brittle deformation. Despite these limitations we have shown that in at least 5 of the 6 regions described, the seismic expression is remarkably consistent with the expectations of flexural strain accumulation. Whereas the prevailing model sees contrasting intermediate depth seismic expression as a consequence of fundamental differences in the slab force balance, our framework suggests they are largely explicable in terms of differences in geometry. This is a significant finding with many ramifications, some of which we discuss more fully below. In so doing, we are not claiming that geometric bending is the only source of stress responsible for slab seismicity. This is clearly not the case. However the recognition that geometric bending plays a significant provides important constraints on slab dynamics from the perspective of slab strength and stress state, in particular.

6.1 Seismicity related to unbending

In reference to Japan, Kawakatsu (1986a) argued that peak rates of geometric unbending were likely to be higher than uniform stretching due to slab pull. Yet it is only in a few regions, northern Japan, Kuriles and Aleutians, where unbending has been recognised as a dominant control on slab seismicity. In particular, with the exception of Isacks and Barazangi (1977), the role of unbending has seldom been discussed in the context of ePac slabs. In this study we have shown that earthquakes consistent with unbending are present in all the wPac and ePac margin slabs, excepting Central America where DC earthquakes seem absent in the putative PUZ. We note, however, that along other sections of the Middle America Trench, DC earthquakes characteristic of unbending are present such as in the Mexican Flat slab region (D. Sandiford et al., 2019). In most cases the PUZ is expressed as a polarised DSZ, with DC earthquakes occurring at shallow levels

580 than a dominantly DT band. These polarised DSZs are consistent with the seismic ex-
581 pression of shortening/extension either side of the neutral plane. However, the propor-
582 tion of DT earthquakes relative to DC in the PUZ is quite variable, as exemplified in the
583 difference between Tonga and Kuriles (Fig. 3a&b). We discuss this variability in the fol-
584 lowing sections.

585 A number of factors make the seismic expression of unbending in ePac slabs less
586 obvious than in wPac slabs. ePac PUZs are shallower than the normal intermediate depth
587 specification (> 70 km) and have often been ignored in studies that follow this somewhat
588 arbitrary designation. Moreover, the close proximity of ePac PUZ events to the megath-
589 rust means that filtering the intraslab earthquakes from the interplate is essential. Fi-
590 nally, at the magnitude range of the CMT catalog, resolving the seismic expression of
591 ePac PUZ requires aggregating seismicity over significant distances.

592 Despite the challenges in resolving the shallow slab seismicity, we are confident that
593 the DSZs we have linked with ePac unbending are robust features. Firstly, we have shown
594 that in Peru and Chile, the DSZs have the correct polarity, and are located precisely where
595 the slab models predict peak rates of curvature reduction (e.g. Fig. 8). Secondly, we are
596 confident that DSZs do comprise intraslab events, rather than grossly mislocated and
597 atypical megathrust or upper plate ruptures. Indeed, the occurrence of isolated DC earth-
598 quakes in the unbending zone in the Nazca plate has been discussed by a number of pre-
599 vious studies. Lemoine et al. (2002) described these as ‘slab push earthquakes’ to dis-
600 tinguish them from what they regarded as the more typical ‘slab pull’ DT earthquakes.
601 Isacks and Barazangi (1977) suggested that DC earthquakes in Peru are related to un-
602 bending, an interpretation that our study supports. Fuenzalida et al. (2013) provide high-
603 resolution aftershock solutions following a medium size DC event in the unbending zone
604 of the Chile slab (Mw 6.1 Michilla Earthquake, Dec. 16, 2007). The aftershock sequence
605 delineates a near-vertical fault plane between about 40 and 50 km depth (likely cross-
606 ing the slab moho). This orientation is consistent with reactivation of a landward-dipping
607 outer-rise normal fault plane, and provides an important insight into the rupture char-
608 acter of a shallow DC unbending event. The identification of a compelling unbending
609 signal in the Nazca plate in Chile and Peru extends the applicability of Kawakatsu’s ar-
610 gument that peak rates of geometric unbending should exceed the background rate of
611 uniform stretching due to slab pull.

6.2 Geometric bending and contrasting seismic expression

In the wPac slab regions we have considered, inferred rates of unbending decay monotonically as slabs straighten in the mid-upper mantle, consistent with a gradual falloff in seismicity rates with depth. Whereas wPac slab morphologies represent a ‘textbook’ view of subduction, ePac slabs are generally more complicated with alternating fully and partially flattened slab sections (Isacks & Barazangi, 1977; Engdahl et al., 1998; Hayes et al., 2018). We argue that these systematic geometric differences are the key control on the contrasting seismic expression of ePac and wPac slabs at intermediate depths. Analysis of the downdip curvature gradient shows that the Nazca plate fully unbends at depths of around 60 km. Beyond this, additional zones of bending are associated with full or partial slab flattening. The majority of ePac DT seismicity is conspicuously clustered in curvature-increasing zones. We summarise these systematic geometric differences between wPac and ePac in Fig. 9.

If geometric bending is the dominant control for localising DT seismicity in ePac slabs, it requires that the lower half of the bending regions (i.e. beneath the neutral plane) is almost completely aseismic. In this light an important observation is that an oppositely polarised DSZ has been observed in microseismicity, near the northern limit of our Chile study region at $\sim 18^\circ\text{S}$ (Comte & Suarez, 1994). In historical catalogues, only a single moderate sized DC earthquake has occurred at intermediate depths in north Chile (17/01/1977 - as labelled in Fig. 5). Using depth phases to precisely constrain the hypocenter, Araujo and Suárez (1994) placed this event about 35 km beneath proximate DT seismicity, consistent with the proposed flexural dynamic state. Indeed, these authors posit that this “inverted” DSZ may be linked to the flexural stresses induced by the change in dip.

These cases notwithstanding, the lack of significant lower plane events in these putative ePac bending zones, like the north Chile seismic belt, may seem at odds with the presence of lower plane events updip in the PUZ. However, this actually follows a pattern that is quite consistent in most subduction settings we analyse. Specifically, it appears that zones of increasing curvature tend to have less lower plane activity compared to zones of decreasing curvature, or unbending. For instance, whereas OBZs tend to have only limited lower plane DC events, PUZs often have more abundant lower plane DT events. One explanation for this is that the flexural stress state is commonly modified by an in-

644 plane component due to slab pull, acting in a sense of effective tension. This is expected
645 to modify the relative depth of the neutral plane of bending (e.g. Mueller et al., 1996;
646 Craig et al., 2014). In zones of increasing curvature, where the flexural stress state in
647 the upper half of the slab is tensional, the addition of in-plane tension shifts the neutral
648 plane deeper, closer to, or even beyond the brittle ductile transition. In zones of decreas-
649 ing curvature, the opposite applies, with the neutral plane shifting towards the slab sur-
650 face into colder parts of the slab, enhancing the prospect of seismic activity beneath the
651 neutral plane.

652 In this context, Tonga is somewhat anomalous in showing a more symmetric pat-
653 tern in the OBZ, with numerous lower plane earthquakes, and a more asymmetric pat-
654 tern in the PUZ with far fewer lower plane earthquakes. This may suggest that, rela-
655 tive to other settings, the magnitude of the uniaxial stress component due to slab pull
656 is significantly reduced or possibly reversed consistent with earlier ideas that Tonga has
657 a more compressive signal than other slab regions (Isacks & Molnar, 1971; Nothard et
658 al., 1996; Gurnis et al., 2000). Alternatively, a significant change in slab strength pro-
659 file may also alter the depth of the neutral plane (e.g. Craig et al., 2014).

660 **6.3 Slab rheology, strain rates and elasticity**

661 At peak slab curvature a purely-elastic differential stress is predicted in the order
662 of 10 GPa. Because this value greatly exceeds inferred yield stresses, inelastic deforma-
663 tion is expected to accommodate the large proportion of bending strains in slabs (Chapple
664 & Forsyth, 1979), with brittle deformation dominating in the cold regions (Goetze & Evans,
665 1979). These predictions are supported by the observation that the cumulative strain
666 of fault throws near the trench (Sleep, 2012), as well as the seismic moment of OBZ earth-
667 quakes (Chapple & Forsyth, 1979) are close to the total strain (rate) inferred from the
668 change in curvature. An important consequence of inelastic deformation is the fact that
669 the flexural stress state is often inverted with respect to the sign of the slab curvature
670 (Engdahl & Scholz, 1977). Indeed the premise that earthquakes occur as a response to
671 slab unbending (where the curvature generally still remains positive) reflects the assump-
672 tion of significant inelastic deformation. When the slab yield strength is low relative to
673 the potential elastic stresses due associated with curvature, the majority of strain is ac-
674 commodated by inelastic deformation, and the flexural stress state will tend to approx-
675 imate the bending rate rather than the curvature. When the sign of the bending rate

676 changes, the flexural stress profile inverts and rapidly saturates with the same polarity
 677 as the bending rate. In this study we have emphasised that, to first order, the orienta-
 678 tion of seismic moment tensors correlates with the inferred bending rate rather than to-
 679 tal strain (i.e. curvature gradient rather than curvature). Overall, our framework sup-
 680 ports the conclusion of numerous previous studies suggesting that comprehensive yield-
 681 ing of slabs must occur throughout the subduction hinge (Engdahl & Scholz, 1977; Goetze
 682 & Evans, 1979; Chapple & Forsyth, 1979; Billen, 2005).

683 **6.4 Implications for subduction dynamics**

684 The sources of buoyancy that drive plate motions are often separated into density
 685 anomalies in the surface plates (e.g. ridges and other topography) and sublithospheric
 686 sources (e.g. slabs, Coblenz et al., 1994; Ghosh et al., 2009). In both cases the scale
 687 of the total anomalous density contribution is relatively well known (Turcotte & Oxburgh,
 688 1967; Afonso et al., 2007), in comparison to uncertainties in the rheology of plates and
 689 mantle. It is the latter that injects substantial complexity and ambiguity in terms in re-
 690 solving how much of the slab density deficit is propagated through slabs to the surface
 691 plates. Attempts to understand the global distribution of plate velocities have concluded
 692 that a large fraction of slab weight must be propagated through the slab (Forsyth & Uyeda,
 693 1975; Conrad & Lithgow-Bertelloni, 2002; van Summeren et al., 2012). While the pres-
 694 ence of intermediate depth DT zones does not constrain the magnitude of stress in slabs,
 695 the suggestion that slabs stretch uniformly is clearly compatible with the idea that stresses
 696 due to slab pull are significant (e.g. Molnar & Bendick, 2019). With simple assumptions
 697 made about effective slab rheology, stresses in the order of 100s of MPa have previously
 698 been estimated (Conrad & Lithgow-Bertelloni, 2004). While the notion that slabs un-
 699 dergo uniform stretching seems consistent with inferences about the forces driving plate
 700 motion, the paradox remains as to why the seismic expression of ‘slab pull’ is evidently
 701 not expressed in wPac slabs, which are attached to the fastest moving large plate.

702 Other lines of evidence suggest slab pull must be significantly smaller than inferred
 703 from plate velocity considerations. Coblenz et al. (1994) argued that the intraplate stress
 704 field is largely explicable in terms of a balance between lithospheric potential-energy dis-
 705 tribution and plate-boundary resistance, implying a relatively low degree of slab-plate
 706 coupling in plates is the norm. These results are implicit in other modelling studies, which
 707 capture the first order features of the intraplate stress field without considering any sub-

708 lithospheric sources (e.g. Ghosh et al. (2009)). Away from trenches, earthquakes in ocean
709 basins mainly show thrust faulting (Sykes & Sbar, 1973), inconsistent with large tensional
710 stress oriented towards subducting slabs. Based on stress indicators in the central In-
711 dian Ocean M. Sandiford et al. (2005) showed that the effective slab pull fraction must
712 be low, around 0.1 in order to account for large magnitude reverse fault mechanisms ob-
713 served in the central Indian Ocean with P-axes parallel to the Sumatran trench, imply-
714 ing an average deviatoric tensional stress no more than order 10 MPa propagated via
715 the slab.

716 The dominant control of bending over stretching in slab seismic strain release is
717 a characteristic of slabs in the Stokes regime, where resistance to slab weight is primar-
718 ily supplied by drag from the mantle (Capitanio et al., 2009; Ribe, 2010; Goes et al., 2011).
719 In this study we highlight the fact slabs in the Stokes regime can develop highly-diverse
720 internal deformation patterns. Indeed, relatively large magnitudes of the curvature gra-
721 dient, and therefore strain rates, can accompany relatively subtle changes in the slab mor-
722 phology, as in northern Chile.

723 A feature of our framework is that it obviates appeals to profound differences in
724 the force balance (or strength) between different slabs, such as is required in the con-
725 ventional interpretation of uniform stretching in Chile, versus shortening in Tonga (e.g.
726 Isacks & Molnar, 1971; Fujita & Kanamori, 1981; P.-F. Chen et al., 2004). In the ge-
727 ometric bending framework, the contrasts in ePac and wPac seismic expression exem-
728 plified by Chile and Tonga arise as a natural consequence of different slab morphology.
729 In the ePac, zones of positive bending rate are associated with full or partial slab flat-
730 tening. Of course, differences in slab morphology will ultimately be an outcome of the
731 subduction force balance. As our numerical models show, however, slabs may evolve very
732 different morphologies while remaining in the Stokes regime. An important implication
733 of our numerical model is the forces required to produce significant changes in slab mor-
734 phology (over millions-of-year periods) can be much smaller than those that would be
735 necessary to produce a transition from flexurally dominated to uniform mode slab de-
736 formation.

737 Recent work suggests that the characteristic ePac/wPac morphology contrasts may
738 be controlled by the interplay between the sinking/retreating slab, and structure of the
739 compensating return flow which tends to determine the upper plate kinematics (Faccenna

740 et al., 2017; Yang et al., 2019). In the ePac margins slab rollback drives a large scale poloidal
741 return flow, in turn promoting fast trench-ward motion of South America and compression-
742 dominated tectonics in the overriding plate. These conditions have been argued to favour
743 flat-slab development along the ePac margin (Manea & Gurnis, 2007; van Hunen et al.,
744 2004; Schellart, 2017; Yang et al., 2019). In contrast, large-scale downwelling beneath
745 Asia, revealed by seismic imaging, geodynamic models, and plate reconstructions restrains
746 trench-ward motion of East Asia. Along with the greater ages of wPac slabs, this pro-
747 motes steeper subduction, extension-dominated upper-plate tectonics, and less flat-slab
748 subduction episodes along the wPac margin (Yang et al., 2019).

749 It is important to note that the numerical model presented here is likely to repre-
750 sent an end member example of subduction in the Stokes regime. The reason is that in
751 the 2d setup, the only significant forces that balance slab buoyancy are mantle drag, plate
752 bending and friction on the subduction interface. When the mantle drag component is
753 largest, the slabs are said to be in the Stokes regime (Ribe, 2010), which is demonstra-
754 bly the case for our model. In 3d mantle convection, slabs and plates interact with other
755 parts of the flow on a range of scales (Hager & O’Connell, 1979). This means that in-
756 dividual plates and slabs are influenced by additional tractions, either basally or along
757 plate boundaries, that may either amplify or resist the slab driven flow. When these ad-
758 ditional forces resist motion toward the subduction zone, the compensation of the slab
759 buoyancy within the mantle is reduced, and larger stresses will be propagated through
760 the subduction hinge to the plate. In a 2d modelling setup, these influences may be re-
761 produced, to a degree, when the plate velocity is fixed by surface boundary conditions
762 (e.g. Sleep, 1979). In this case, when the mantle viscosity is reduced, the slab is unable
763 to respond with a proportionate increase its sinking rate. The mantle drag is reduced,
764 a greater component of the slab buoyancy is propagated through the slab to the plate,
765 and the component of uniform stretching, relative to geometric bending is thus increased
766 (Sleep, 1979). An end member in this type of setup occurs when the velocity of the sur-
767 face plates is zero, and the attached slab will predominately undergo necking in the as-
768 thenosphere.

769 Following the thread of the preceding paragraph, our framework provides an in-
770 teresting perspective on the dynamics of intra-continental intermediate depth seismic zones.
771 High seismic strain rates ($10^{-14} s^{-1}$) have been inferred in the Hindu Kush and the Vrancea
772 zone beneath the Carpathians (Lorinczi & Houseman, 2009; Molnar & Bendick, 2019).

773 These are an order of magnitude greater than typical intermediate depth seismic strain
 774 in subducting slabs ($\sim 10^{-15} s^{-1}$). The strain rates beneath the Hindu Kush and Vrancea
 775 may indicate deformation dominated by lithospheric necking (e.g. uniform stretching Lis-
 776 ter et al., 2008; Lorinczi & Houseman, 2009). Meanwhile, as we have argued, earthquakes
 777 in Pacific margin subduction zones reflect rates imposed by geometric bending consis-
 778 tent with the observed seismic release rates closer to $10^{-15} s^{-1}$ (Kawakatsu, 1986a; Nothard
 779 et al., 1996).

780 **6.5 Limitations and future work**

781 In investigating the potential signal of flexure in slab seismicity, we have focused
 782 on the geometric (or advective) component of the bending rate (Ribe, 2001, 2010; Buf-
 783 fett, 2006). The time-independence allows us to infer the relative variation in long-term
 784 bending rates from present day slab geometry. The geometric component should be the
 785 dominant bending term for slabs in which: a) the hinge morphology is not changing rapidly,
 786 and b) our of plane contributions to the stress/deformation are relatively minor (Buffett
 787 & Becker, 2012). Clearly these conditions will not be met in all slab regions, and this
 788 caveat will require careful attention in trying to test this hypothesis in other settings.
 789 In this study we have primarily focused on the variation in the orientation of moment
 790 tensors with respect to slab geometry in general, especially the curvature gradient. We
 791 have been more circumspect about the correlation between seismicity rates and the rel-
 792 ative magnitude of the curvature gradient. This is primarily because seismic activity rates
 793 are not necessarily proportional to the long term strain rate (i.e. the bending rates in-
 794 ferred via the curvature gradient). The influence of metamorphic processes, and distri-
 795 bution of fluids, in subducting slabs is likely to influence the rates of seismicity. For ex-
 796 ample, Boneh et al. (2019) have shown that the intermediate depth seismic activity rate
 797 varies with the inferred amount of plate hydration in the outer-rise region, with simi-
 798 lar mechanisms being linked to rapid changes seismic expression along-strike (Shillington
 799 et al., 2015). Such process may explain the very different seismic activity rates in the
 800 north Chile seismic belt, compared with the Nazca slab further south (e.g. Fig. 4a). An-
 801 other factor is the increasing role of ductile deformation as the slab heats up from above
 802 and below. As a result, the relative amount of seismic/ductile deformation is likely to
 803 vary in a complex manner with changes in pressure and temperature. Finally, short cat-
 804 alog times also bias the relative number of earthquakes in different parts of the slab. We

805 highlight, for instance, the increase in OBZ seismicity in Northern Japan following the
806 Tohoku earthquake.

807 As noted in Section 5, there are number of instances where the correlation between
808 curvature gradient and seismic expression is ambiguous, absent, or opposite to expect-
809 ations for a primary geometric bending control. We briefly discuss these below, some
810 of which are readily explained, and some not. In the ePac settings, several clusters of
811 seismicity are likely to be unrelated to downdip geometric bending. The Pucallpa seis-
812 mic nest in Chile appears to be spatially correlated with a relatively localised lateral per-
813 turbation of the slab morphology (Gutscher et al., 2000; Wagner & Okal, 2019) and it
814 is reasonable to assume that these features are related. While for Chile we demonstrate
815 a close spatial association between the main peak in positive curvature gradient (see Fig.
816 8a) and the primary cluster of DT seismicity (the north Chile seismic belt, see Fig. 4a),
817 the relationship is less evident at greater depths. Based on our geometric analysis, the
818 slab would be expected to go through an additional zone of unbending (i.e. a secondary
819 unbending zone), where the sign of the curvature gradient returns to negative (e.g. Fig.
820 8a) in analogous fashion to our numerical model, which predicts a return to downdip short-
821 ening at around 550 km from the trench (RHS of lower panel in Fig. 6). Instead, the in-
822 termediate depth seismicity beneath 150 km remains dominated by DT axes. As we have
823 noted, this deeper cluster is unusual in that it forms a nearly continuous, steeply dip-
824 ping band that shallows toward the south (as shown in supplementary Fig. S6).

825 The apparent absence of deep DC earthquakes associated with upper plane unbend-
826 ing at the expected depth-distance range in ePac slabs, may signal the slab stress de-
827 formation state transitions from flexurally-dominated to a more prominent uniaxial com-
828 ponent (Bloch et al., 2018). Alternatively, progressive warming of the upper part of the
829 slab and/or processes related to dehydration, may leave it essentially aseismic at these
830 depths, with the consequence that the seismically active zone lies beneath the midplane.
831 These points highlight an important caveat in our ability to relate earthquake hypocen-
832 ters accurately within a geometric framework, as seismicity still provides the best con-
833 straint on the geometry. Uncertainties in both hypocentral locations and slab models are
834 significant and require ongoing work.

7 Conclusions

Our study suggests that flexural deformation plays a significant role in the seismic expression of subducting slabs. We have analysed the contribution of the geometric bending rate, and found that in several key locations, the orientation of slab seismic moment tensors vary systematically with the anticipated sense of deformation. The fact that flexure controls seismicity patterns in the OBZ is of course, already widely accepted, as is the effect of unbending in a limited number of slab settings. In terms of extending the role of bending/unbending, our contributions are twofold. Firstly we show that seismicity characteristic of unbending is prevalent in ePac slabs, albeit at shallower depths than wPac slabs. We then show that geometric differences between ePac and wPac slabs lead to additional zones of bending at intermediate depths in ePac slabs. The majority of ePac DT seismicity is conspicuously clustered in these curvature-increasing zones, which are associated with full or partial slab flattening. Hence, the contrasting seismic expression of ePac and wPac slabs appears to arise due to systematic differences in slab morphology rather than differences in in-plane stress associated with either uniform downdip extension in the former or shortening in the latter. The observed correlation of earthquake T-axes orientations with the curvature gradient, rather than the curvature, arises from the fact that a very significant proportion of flexural strain is accommodated by inelastic deformation, of which seismic slip itself is a key component. The seismic expression of flexure is strongly modified by the relative contribution of brittle deformation above and below the neutral plane. Within the time frame of historical catalogues, this may range from abundant seismicity in both planes (i.e. the Kuriles PUZ) to virtually no seismicity in the lower plane (i.e. the north Chile seismic belt). A simple qualitative explanation is that the depth of the neutral plane exhibits variability with respect to the thermal structure of slabs, with the latter defining the transition from dominantly brittle to dominantly ductile deformation.

861 **Acknowledgments**

862 This work was supported by the Australian Research council (Discovery grant DP150102887).
 863 Development of the Underworld2 code (<http://www.underworldcode.org/>) was supported
 864 by AuScope. DS's postgraduate research at the University of Melbourne was supported
 865 by a Baragwanath Geology Research Scholarship. This work was supported by resources
 866 provided by The Pawsey Supercomputing Centre with funding from the Australian Gov-
 867 ernment and the Government of Western Australia. This work was supported by the Nec-
 868 tar Research Cloud, a collaborative Australian research platform supported by the Na-
 869 tional Collaborative Research Infrastructure Strategy (NCRIS). The study benefited from
 870 discussions and reviews by Greg Houseman, Claire Currie, Norman Sleep and Laurent
 871 Jolivet.

872 **References**

- 873 Afonso, J., Ranalli, G., & Fernandez, M. (2007). Density structure and buoyancy of
 874 the oceanic lithosphere revisited. *Geophysical Research Letters*, *34*(10).
- 875 Agrusta, R., Goes, S., & van Hunen, J. (2017). Subducting-slab transition-zone
 876 interaction: Stagnation, penetration and mode switches. *Earth and Planetary
 877 Science Letters*, *464*, 10–23.
- 878 Araujo, M., & Suárez, G. (1994). Geometry and state of stress of the subducted
 879 nazca plate beneath central chile and argentina: evidence from teleseismic
 880 data. *Geophysical Journal International*, *116*(2), 283–303.
- 881 Bailey, I. W., Becker, T. W., & Ben-Zion, Y. (2009). Patterns of co-seismic strain
 882 computed from southern California focal mechanisms. *Geophysical Journal In-
 883 ternational*, *177*(3), 1015–1036.
- 884 Barazangi, M., & Isacks, B. (1976). Spatial distribution of earthquakes and subduc-
 885 tion of the Nazca plate beneath South America. *Geology*, *4*(11), 686.
- 886 Billen, M. I. (2005). Constraints on subducting plate strength within the Kermadec
 887 trench. *Journal of Geophysical Research*, *110*(B5).
- 888 Billen, M. I., Gurnis, M., & Simons, M. (2003). Multiscale dynamics of the Tonga-
 889 Kermadec subduction zone. *Geophysical Journal International*, *153*(2), 359–
 890 388.
- 891 Bloch, W., Schurr, B., Kummerow, J., Salazar, P., & Shapiro, S. A. (2018). From
 892 slab coupling to slab pull: Stress segmentation in the subducting Nazca plate.

- 893 *Geophysical Research Letters*, 45(11), 5407–5416.
- 894 Boneh, Y., Schottenfels, E., Kwong, K., Zelst, I., Tong, X., Eimer, M., ... Zhan, Z.
895 (2019). Intermediate-depth earthquakes controlled by incoming plate hydration
896 along bending-related faults. *Geophysical Research Letters*, 46(7), 3688–3697.
- 897 Brudzinski, M. R., Thurber, C. H., Hacker, B. R., & Engdahl, E. R. (2007). Global
898 prevalence of double benioff zones. *Science*, 316(5830), 1472–1474.
- 899 Buffett, B. A. (2006). Plate force due to bending at subduction zones. *Journal of*
900 *Geophysical Research*, 111(B9).
- 901 Buffett, B. A., & Becker, T. W. (2012). Bending stress and dissipation in subducted
902 lithosphere. *Journal of Geophysical Research*, 117(B5).
- 903 Caldwell, J., Haxby, W., Karig, D. E., & Turcotte, D. (1976). On the applicability of
904 a universal elastic trench profile. *Earth and Planetary Science Letters*, 31(2),
905 239–246.
- 906 Capitanio, F., Morra, G., & Goes, S. (2007). Dynamic models of downgoing plate-
907 buoyancy driven subduction: Subduction motions and energy dissipation.
908 *Earth and Planetary Science Letters*, 262(1-2), 284–297.
- 909 Capitanio, F., Morra, G., & Goes, S. (2009). Dynamics of plate bending at the
910 trench and slab-plate coupling. *Geochemistry, Geophysics, Geosystems*, 10(4).
- 911 Chapple, W. M., & Forsyth, D. W. (1979). Earthquakes and bending of plates at
912 trenches. *Journal of Geophysical Research: Solid Earth*, 84(B12), 6729–6749.
- 913 Chen, M., Manea, V. C., Niu, F., Wei, S. S., & Kiser, E. (2019). Genesis of
914 intermediate-depth and deep intraslab earthquakes beneath Japan constrained
915 by seismic tomography, seismicity, and thermal modeling. *Geophysical Re-*
916 *search Letters*, 46(4), 2025–2036.
- 917 Chen, P.-F., Bina, C. R., & Okal, E. A. (2004). A global survey of stress orienta-
918 tions in subducting slabs as revealed by intermediate-depth earthquakes. *Geo-*
919 *physical Journal International*, 159(2), 721–733.
- 920 Coblentz, D. D., Richardson, R. M., & Sandiford, M. (1994). On the gravitational
921 potential of the Earth’s lithosphere. *Tectonics*, 13(4), 929–945.
- 922 Comte, D., Dorbath, L., Pardo, M., Monfret, T., Haessler, H., Rivera, L., ... Mene-
923 ses, C. (1999). A double-layered seismic zone in Arica, northern Chile. *Geo-*
924 *physical Research Letters*, 26(13), 1965–1968.
- 925 Comte, D., & Suarez, G. (1994). An inverted double seismic zone in Chile: Evidence

- 926 of phase transformation in the subducted slab. *Science*, *263*(5144), 212–215.
- 927 Conrad, C. P., & Lithgow-Bertelloni, C. (2002). How mantle slabs drive plate tec-
928 tonics. *Science*, *298*(5591), 207–209.
- 929 Conrad, C. P., & Lithgow-Bertelloni, C. (2004). The temporal evolution of plate
930 driving forces: Importance of “slab suction” versus “slab pull” during the
931 Cenozoic. *Journal of Geophysical Research: Solid Earth*, *109*(B10).
- 932 Craig, T. J., Copley, A., & Jackson, J. (2014). A reassessment of outer-rise seis-
933 micity and its implications for the mechanics of oceanic lithosphere. *Geophys-
934 ical Journal International*, *197*(1), 63–89.
- 935 Ekström, G., Nettles, M., & Dziewoński, A. (2012). The global CMT project
936 2004–2010: Centroid-moment tensors for 13, 017 earthquakes. *Physics of the
937 Earth and Planetary Interiors*, *200-201*, 1–9.
- 938 Elsasser, W. M. (1969). Convection and stress propagation in the upper mantle.
- 939 Emmerson, B., & McKenzie, D. (2007). Thermal structure and seismicity of sub-
940 ducting lithosphere. *Physics of the Earth and Planetary Interiors*, *163*(1-4),
941 191–208.
- 942 Engdahl, E. R., & Scholz, C. H. (1977). A double Benioff Zone beneath the cen-
943 tral Aleutians: An unbending of the lithosphere. *Geophysical Research Letters*,
944 *4*(10), 473–476.
- 945 Engdahl, E. R., van der Hilst, R., & Buland, R. (1998). Global teleseismic earth-
946 quake relocation with improved travel times and procedures for depth determi-
947 nation. *Bulletin of the Seismological Society of America*, *88*(3), 722–743.
- 948 Faccenda, M. (2014). Water in the slab: A trilogy. *Tectonophysics*, *614*, 1–30.
- 949 Faccenna, C., Oncken, O., Holt, A. F., & Becker, T. W. (2017). Initiation of the
950 andean orogeny by lower mantle subduction. *Earth and Planetary Science Let-
951 ters*, *463*, 189–201.
- 952 Forsyth, D., & Uyeda, S. (1975). On the relative importance of the driving forces of
953 plate motion. *Geophysical Journal International*, *43*(1), 163–200.
- 954 Fuenzalida, A., Schurr, B., Lancieri, M., Sobiesiak, M., & Madariaga, R. (2013).
955 High-resolution relocation and mechanism of aftershocks of the 2007 Tocopilla
956 (Chile) earthquake. *Geophysical Journal International*, *194*(2), 1216–1228.
- 957 Fujita, K., & Kanamori, H. (1981). Double seismic zones and stresses of intermedi-
958 ate depth earthquakes. *Geophysical Journal International*, *66*(1), 131–156.

- 959 Garel, F., Goes, S., Davies, D., Davies, J. H., Kramer, S. C., & Wilson, C. R.
 960 (2014). Interaction of subducted slabs with the mantle transition-zone: A
 961 regime diagram from 2-d thermo-mechanical models with a mobile trench and
 962 an overriding plate. *Geochemistry, Geophysics, Geosystems*, 15(5), 1739–1765.
- 963 Ghosh, A., Holt, W. E., & Flesch, L. M. (2009). Contribution of gravitational po-
 964 tential energy differences to the global stress field. *Geophysical Journal Inter-
 965 national*, 179(2), 787–812.
- 966 Goes, S., Capitanio, F., Morra, G., Seton, M., & Giardini, D. (2011). Signatures
 967 of downgoing plate-buoyancy driven subduction in Cenozoic plate motions.
 968 *Physics of the Earth and Planetary Interiors*, 184(1-2), 1–13.
- 969 Goetze, C., & Evans, B. (1979). Stress and temperature in the bending lithosphere
 970 as constrained by experimental rock mechanics. *Geophysical Journal Interna-
 971 tional*, 59(3), 463–478.
- 972 Green, H. W., & Houston, H. (1995). The mechanics of deep earthquakes. *Annual
 973 Review of Earth and Planetary Sciences*, 23(1), 169–213.
- 974 Gurnis, M., Ritsema, J., Heijst, H.-J. V., & Zhong, S. (2000). Tonga slab de-
 975 formation: The influence of a lower mantle upwelling on a slab in a young
 976 subduction zone. *Geophysical Research Letters*, 27(16), 2373–2376.
- 977 Gutenberg, B., & Richter, C. (1954). *Seismicity of the world and associated phenom-
 978 ena*. Princeton University Press, Princeton, NJ.
- 979 Gutscher, M.-A., Spakman, W., Bijwaard, H., & Engdahl, E. R. (2000). Geody-
 980 namics of flat subduction: Seismicity and tomographic constraints from the
 981 Andean margin. *Tectonics*, 19(5), 814–833.
- 982 Hacker, B. R., Peacock, S. M., Abers, G. A., & Holloway, S. D. (2003). Subduction
 983 factory 2. are intermediate-depth earthquakes in subducting slabs linked to
 984 metamorphic dehydration reactions? *Journal of Geophysical Research: Solid
 985 Earth*, 108(B1).
- 986 Hager, B. H., & O’Connell, R. J. (1979). Kinematic models of large-scale flow in the
 987 earth’s mantle. *Journal of Geophysical Research: Solid Earth*, 84(B3), 1031–
 988 1048.
- 989 Hasegawa, A., Umino, N., & Takagi, A. (1978). Double-planed structure of the deep
 990 seismic zone in the northeastern Japan arc. *Tectonophysics*, 47(1-2), 43–58.
- 991 Hayes, G. P., Moore, G. L., Portner, D. E., Hearne, M., Flamme, H., Furtney, M.,

- 992 & Smoczyk, G. M. (2018). Slab2, a comprehensive subduction zone geometry
993 model. *Science*, *362*(6410), 58–61.
- 994 Hayes, G. P., Wald, D. J., & Johnson, R. L. (2012). Slab1.0: A three-dimensional
995 model of global subduction zone geometries. *Journal of Geophysical Research:*
996 *Solid Earth*, *117*(B1).
- 997 House, L. S., & Jacob, K. H. (1982). Thermal stresses in subducting lithosphere can
998 explain double seismic zones. *Nature*, *295*(5850), 587–589.
- 999 Imanishi, K., Ando, R., & Kuwahara, Y. (2012). Unusual shallow normal-faulting
1000 earthquake sequence in compressional northeast japan activated after the 2011
1001 off the pacific coast of tohoku earthquake. *Geophysical Research Letters*, *39*(9).
1002 doi: 10.1029/2012gl051491
- 1003 Isacks, B., & Barazangi, M. (1977). Geometry of benioff zones: Lateral segmentation
1004 and downwards bending of the subducted lithosphere. In *Island arcs, deep sea*
1005 *trenches and back-arc basins* (pp. 99–114). American Geophysical Union.
- 1006 Isacks, B., & Molnar, P. (1969). Mantle Earthquake Mechanisms and the Sinking of
1007 the Lithosphere. *Nature*, *223*(5211), 1121–1124.
- 1008 Isacks, B., & Molnar, P. (1971). Distribution of stresses in the descending litho-
1009 sphere from a global survey of focal-mechanism solutions of mantle earth-
1010 quakes. *Review of Geophysics*, *9*(1), 103.
- 1011 Kawakatsu, H. (1986a). Double seismic zones: Kinematics. *Journal of Geophysical*
1012 *Research*, *91*(B5), 4811.
- 1013 Kawakatsu, H. (1986b). Downdip tensional earthquakes beneath the Tonga Arc: A
1014 double seismic zone? *Journal of Geophysical Research*, *91*(B6), 6432.
- 1015 Kirby, S., Engdahl, R. E., & Denlinger, R. (2013). Intermediate-depth intraslab
1016 earthquakes and arc volcanism as physical expressions of crustal and upper-
1017 most mantle metamorphism in subducting slabs. In *Subduction top to bottom*
1018 (pp. 195–214). American Geophysical Union.
- 1019 Kita, S., Okada, T., Hasegawa, A., Nakajima, J., & Matsuzawa, T. (2010). Exis-
1020 tence of interplane earthquakes and neutral stress boundary between the upper
1021 and lower planes of the double seismic zone beneath Tohoku and Hokkaido,
1022 northeastern Japan. *Tectonophysics*, *496*(1-4), 68–82.
- 1023 Lemoine, A., Madariaga, R., & Campos, J. (2002). Slab-pull and slab-push earth-
1024 quakes in the Mexican, Chilean and Peruvian subduction zones. *Physics of the*

- 1025 *Earth and Planetary Interiors*, 132(1-3), 157–175.
- 1026 Lister, G., Kennett, B., Richards, S., & Forster, M. (2008). Boudinage of a stretch-
1027 ing slablet implicated in earthquakes beneath the Hindu Kush. *Nature Geo-*
1028 *science*, 1(3), 196.
- 1029 Lorinczi, P., & Houseman, G. (2009). Lithospheric gravitational instability beneath
1030 the Southeast Carpathians. *Tectonophysics*, 474(1-2), 322–336.
- 1031 Manea, V., & Gurnis, M. (2007). Subduction zone evolution and low viscosity
1032 wedges and channels. *Earth and Planetary Science Letters*, 264(1-2), 22–45.
- 1033 McKenzie, D. P. (1969). Speculations on the consequences and causes of plate mo-
1034 tions. *Geophysical Journal International*, 18(1), 1–32.
- 1035 Molnar, P., & Bendick, R. (2019). Seismic moments of intermediate-depth earth-
1036 quakes beneath the Hindu Kush: Active stretching of a blob of sinking thick-
1037 ened mantle lithosphere? *Tectonics*, 38, 1651–1665.
- 1038 Mueller, S., Spence, W., & Choy, G. L. (1996). Inelastic models of lithospheric
1039 stress-11. implications for outer-rise seismicity and dynamics. *Geophysical*
1040 *Journal International*, 125(1), 54–72.
- 1041 Nothard, S., McKenzie, D., Haines, J., & Jackson, J. (1996). Gaussian curvature
1042 and the relationship between the shape and the deformation of the Tonga slab.
1043 *Geophysical Journal International*, 127(2), 311–327.
- 1044 Peacock, S. M. (2001). Are the lower planes of double seismic zones caused by ser-
1045 pentine dehydration in subducting oceanic mantle? *Geology*, 29(4), 299.
- 1046 Ribe, N. M. (2001). Bending and stretching of thin viscous sheets. *Journal of Fluid*
1047 *Mechanics*, 433, 135–160.
- 1048 Ribe, N. M. (2010). Bending mechanics and mode selection in free subduction: a
1049 thin-sheet analysis. *Geophysical Journal International*, 180(2), 559–576.
- 1050 Richter, F. M. (1979). Focal mechanisms and seismic energy release of deep and
1051 intermediate earthquakes in the Tonga-Kermadec Region and their bearing on
1052 the depth extent of mantle flow. *Journal of Geophysical Research: Solid Earth*,
1053 84(B12), 6783–6795.
- 1054 Rietbrock, A., & Waldhauser, F. (2004). A narrowly spaced double-seismic zone in
1055 the subducting Nazca plate. *Geophysical Research Letters*, 31(10), n/a–n/a.
- 1056 Romeo, I., & Álvarez-Gómez, J. (2018). Lithospheric folding by flexural slip in sub-
1057 duction zones as source for reverse fault intraslab earthquakes. *Scientific re-*

- 1058 *ports*, 8(1), 1367.
- 1059 Rosenbaum, G., Sandiford, M., Caulfield, J., & Garrison, J. M. (2019). A trapdoor
1060 mechanism for slab tearing and melt generation in the northern Andes. *Geol-*
1061 *ogy*, 47(1), 23–26.
- 1062 Russo, R., & Silver, P. (1994). Trench-parallel flow beneath the nazca plate from
1063 seismic anisotropy. *Science*, 263(5150), 1105–1111.
- 1064 Samowitz, I. R., & Forsyth, D. W. (1981). Double seismic zone beneath the Mariana
1065 Island Arc. *Journal of Geophysical Research*, 86(B8), 7013–7021.
- 1066 Sandiford, D., & Moresi, L. (2019). Improving subduction interface implementation
1067 in dynamic numerical models. *Solid Earth*, 10(3), 969–985.
- 1068 Sandiford, D., Moresi, L., Sandiford, M., & Yang, T. (2019). Geometric controls on
1069 flat slab seismicity. *Earth and Planetary Science Letters*, 527, 115787.
- 1070 Sandiford, M., Coblenz, D., & Schellart, W. P. (2005). Evaluating slab-plate cou-
1071 pling in the Indo-Australian plate. *Geology*, 33(2), 113.
- 1072 Schellart, W. P. (2004). Quantifying the net slab pull force as a driving mechanism
1073 for plate tectonics. *Geophysical Research Letters*, 31(7), L07611.
- 1074 Schellart, W. P. (2017). Andean mountain building and magmatic arc migration
1075 driven by subduction-induced whole mantle flow. *Nature communications*,
1076 8(1), 2010.
- 1077 Seno, T., & Yamanaka, Y. (2013). Double seismic zones, compressional deep trench-
1078 outer rise events, and superplumes. In *Subduction top to bottom* (pp. 347–355).
1079 American Geophysical Union.
- 1080 Shillington, D. J., Bécel, A., Nedimović, M. R., Kuehn, H., Webb, S. C., Abers,
1081 G. A., ... Mattei-Salicrup, G. A. (2015). Link between plate fabric, hydration
1082 and subduction zone seismicity in Alaska. *Nature Geoscience*, 8(12), 961.
- 1083 Sleep, N. H. (1979). The double seismic zone in downgoing slabs and the viscosity of
1084 the mesosphere. *Journal of Geophysical Research*, 84(B9), 4565.
- 1085 Sleep, N. H. (2012). Constraint on the recurrence of great outer-rise earthquakes
1086 from seafloor bathymetry. *Earth, Planets and Space*, 64(12), 19.
- 1087 Sykes, L. R., & Sbar, M. L. (1973). Intraplate earthquakes, lithospheric stresses and
1088 the driving mechanism of plate tectonics. *Nature*, 245(5424), 298–302.
- 1089 Tsujimori, T., Sisson, V., Liou, J., Harlow, G., & Sorensen, S. (2006). Very-low-
1090 temperature record of the subduction process: A review of worldwide lawsonite

- 1091 eclogites. *Lithos*, 92(3-4), 609–624.
- 1092 Tsukahara, H. (1980). Physical conditions for double seismic planes of the deep seis-
1093 mic zone. *Journal of Physics of the Earth*, 28(1), 1–15.
- 1094 Turcotte, D., & Oxburgh, E. (1967). Finite amplitude convective cells and continen-
1095 tal drift. *Journal of Fluid Mechanics*, 28(1), 29–42.
- 1096 van Hunen, J., van den Berg, A. P., & Vlaar, N. J. (2004). Various mechanisms to
1097 induce present-day shallow flat subduction and implications for the younger
1098 Earth: a numerical parameter study. *Physics of the Earth and Planetary*
1099 *Interiors*, 146(1-2), 179–194.
- 1100 van Summeren, J., Conrad, C. P., & Lithgow-Bertelloni, C. (2012). The importance
1101 of slab pull and a global asthenosphere to plate motions. *Geochemistry, Geo-*
1102 *physics, Geosystems*, 13(2).
- 1103 Vassiliou, M., Hager, B., & Raefsky, A. (1984). The distribution of earthquakes with
1104 depth and stress in subducting slabs. *Journal of Geodynamics*, 1(1), 11–28.
- 1105 Wagner, L. S., & Okal, E. A. (2019). The Pucallpa Nest and its constraints on the
1106 geometry of the Peruvian Flat Slab. *Tectonophysics*, 762, 97–108.
- 1107 Wang, K. (2002). Unbending combined with dehydration embrittlement as a cause
1108 for double and triple seismic zones. *Geophysical Research Letters*, 29(18), 36–
1109 1–36–4.
- 1110 Yang, T., Gurnis, M., & Zhan, Z. (2017). Trench motion-controlled slab morphology
1111 and stress variations: Implications for the isolated 2015 Bonin Islands deep
1112 earthquake. *Geophysical Research Letters*, 44(13), 6641–6650.
- 1113 Yang, T., Moresi, L., Gurnis, M., Liu, S., Sandiford, D., Williams, S., & Capitanio,
1114 F. A. (2019). Contrasted East Asia and South America tectonics driven by
1115 deep mantle flow. *Earth and Planetary Science Letters*, 517, 106–116.

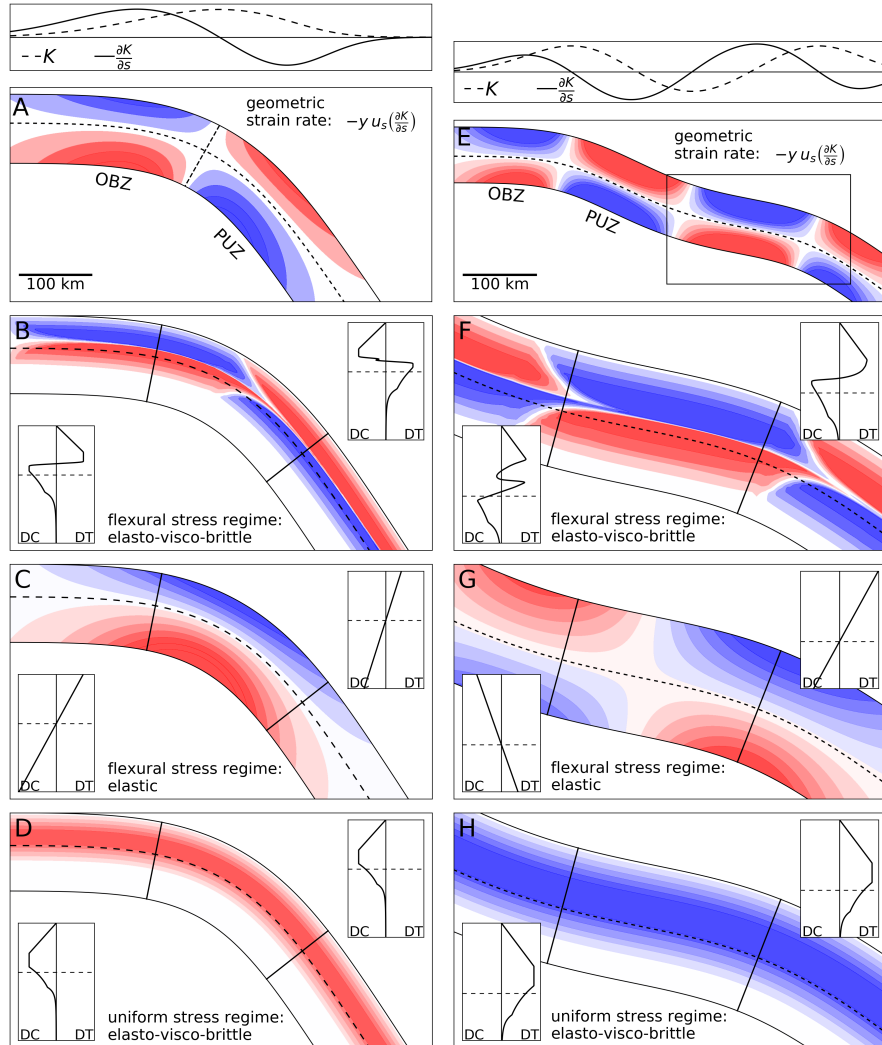


Figure 1: Schematic illustration of key geometrical/mechanical concepts motivating our analysis of the seismic expression of subducting slabs. Left side - typical west Pacific style subduction geometry as represented for example by Tonga. Right side - typical east Pacific style subduction geometry as represented for example by Chile. A,E top panel - slab midplane curvature (dashed) and curvature gradient (solid). A,E bottom panel - geometric strain rate. Box in E shows areas enlarged in F-H. B,F stress distribution for a elasto-plasto-viscous rheology deforming in by flexural bending. C,G - stress distribution for an elastic rheology deforming by geometric bending. D,H - stress distribution for for a elasto-visco-plastic rheology deforming in response to uniform downdip compression (left) and extension (right). Insets show schematic differential stress profiles across the slab, as marked by solid black line with positive values implying extension.

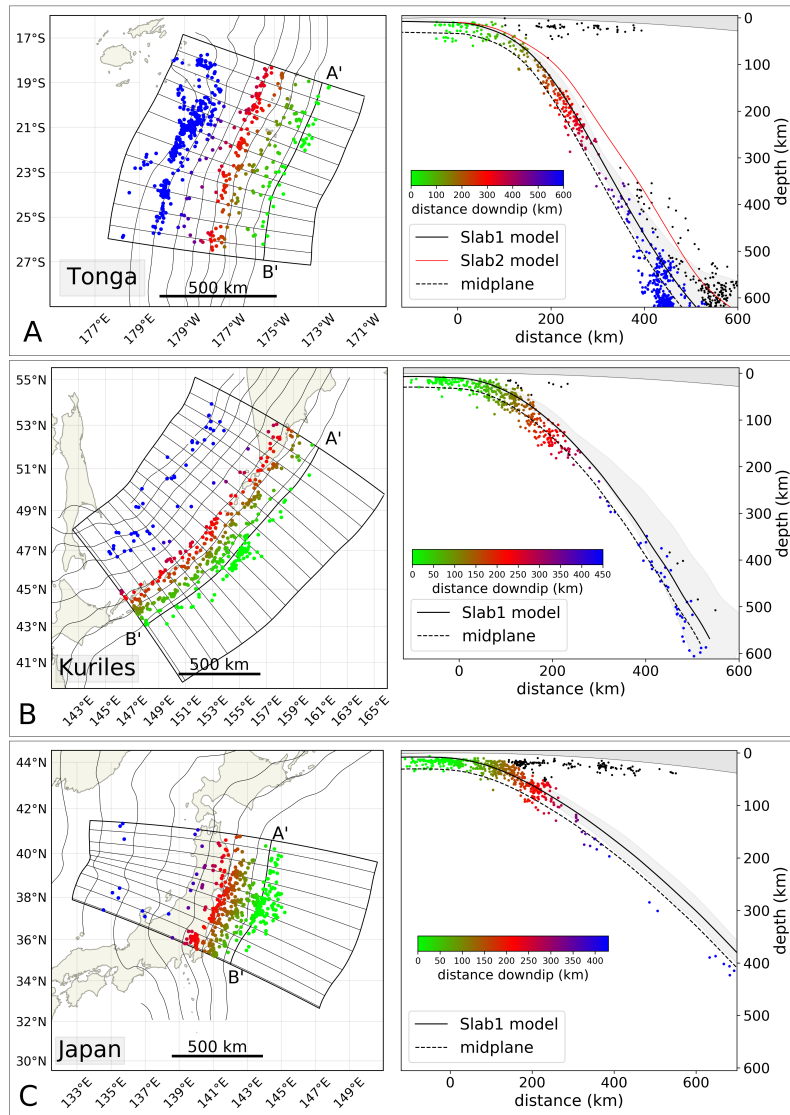


Figure 2: Overview of western Pacific margin slab segments analysed in this study. Colored points show intraslab seismicity which is consistent with best available slab geometry model (e.g. Slab1 for Tonga). Earthquakes lying more than 20 km above the slab surface, shown as small black points, are considered upper-plate events, outliers (presumably due to depth error), or regions where our slab models do not properly resolve the local slab morphology, and so along with earthquakes identified as likely megathrust ruptures (not shown) are excluded from our analysis. Left hand panels show slab earthquakes in map view. Right hand panels shows projection of the earthquakes on a trench-parallel cross section: the solid black line shows the region-averaged slab surface model; the gray region shows the lateral variation in slab surface model across the domain; the dashed black line shows the slab midplane (an orthogonal translation of the slab surface, as discussed in the supplementary material); the red dashed line shows the Slab2 model for Tonga, which shows less consistency with the earthquake hypocenters (ISC-EHB catalog).

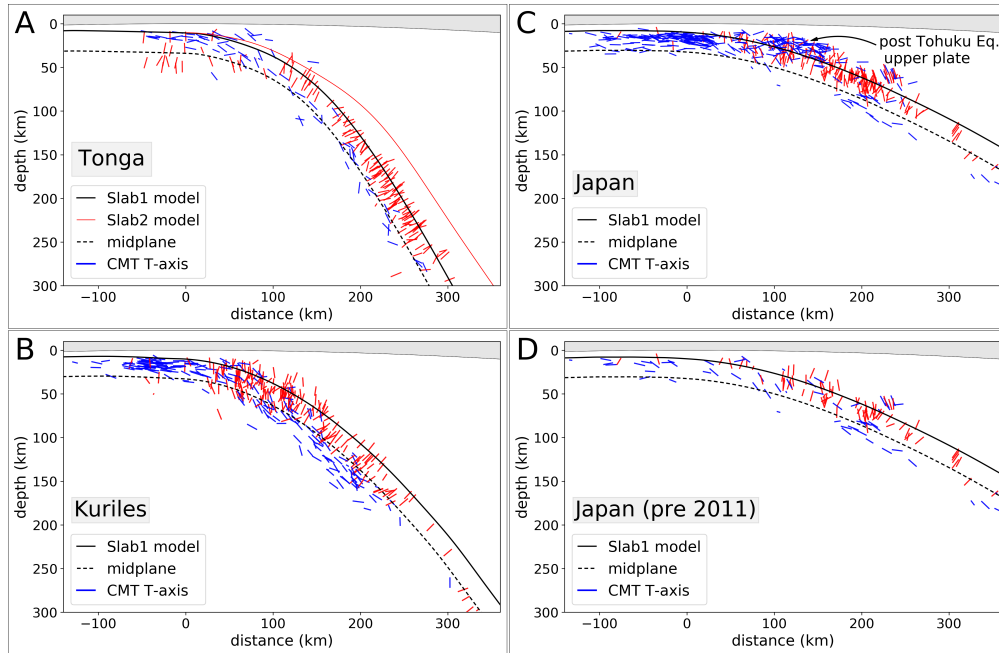


Figure 3: wPac trench-perpendicular projection of CMT T-axes (ISC-EHB hypocenters) on a vertical cross-sections, along the nearest trench normal azimuthal lines shown Fig. 2, with data aggregated across the entire domain. The origin of the horizontal axis represents the trench location. The T-axes are plotted as projections of uniform-length vectors, with the length variation in the plotted T-axes reflecting the magnitude of the projected component of the vector. T-axes are coloured according to the orientation relative to the slab midplane (shown with dashed black line): red represents earthquakes with a DC sense, blue with a DT sense.

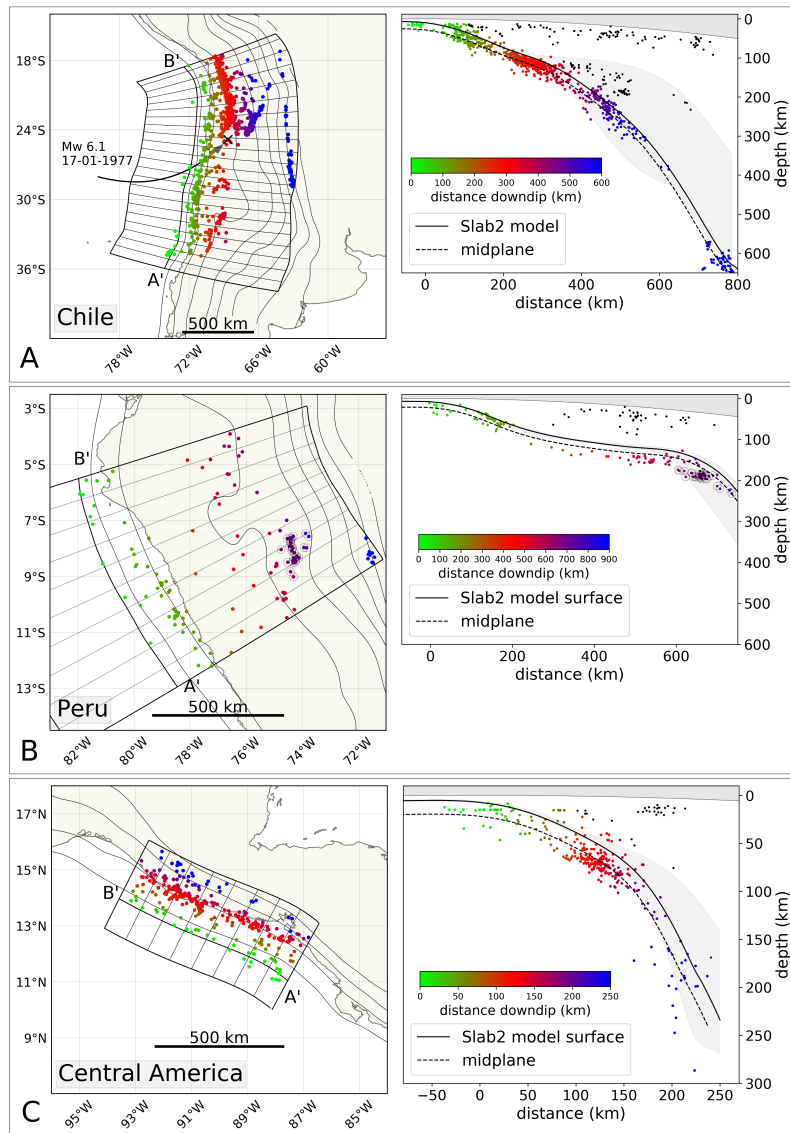


Figure 4: Overview of eastern Pacific margin slab segments analysed in this study. See Fig. 2 caption for details of figure organisation and preparation. The black points represent earthquakes that lie more the 20 km above the slab surface model. For Chile, these mainly represents the relatively small number of earthquakes that occur in close proximity to the Pampean flat slab in the south, where the slab morphology is quite different to northern Chile. In B, the Pucallpa nest earthquakes are indicated by open circles (as discussed in the main text).

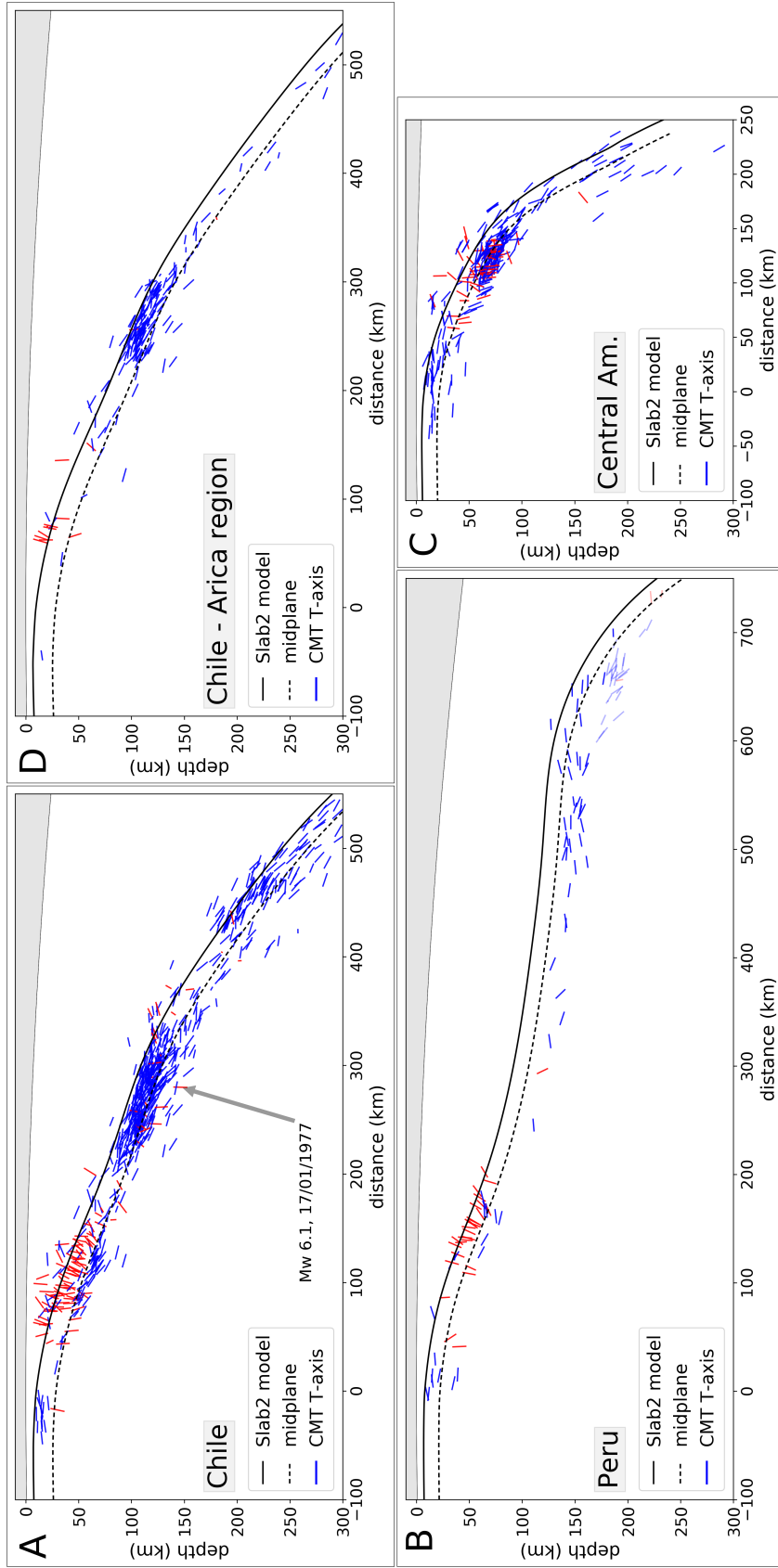


Figure 5: ePac slab profile sections. See Fig. 3 caption for details of figure organisation and preparation.

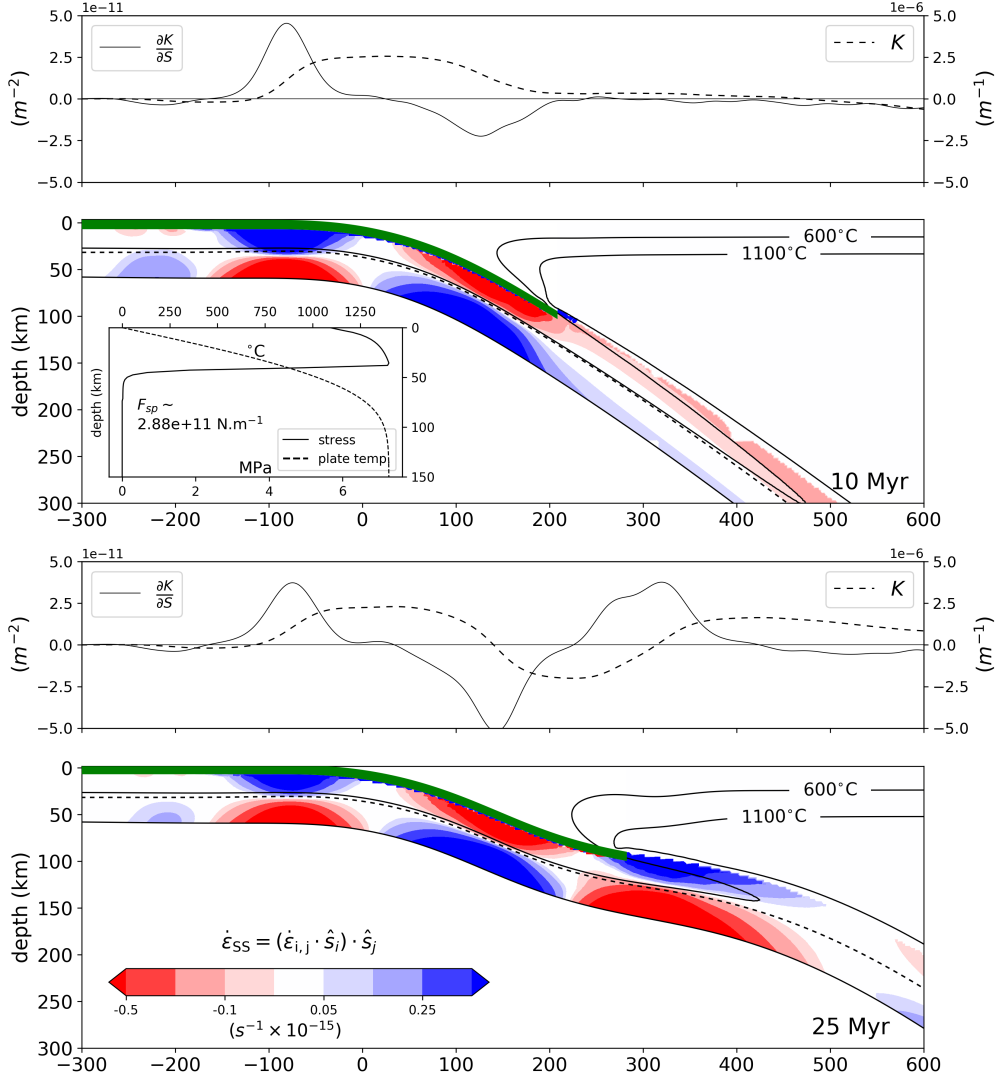


Figure 6: Strain rate distribution in numerical model at 10 Myr and 25 Myr. For each figure the main panel shows the down-dip strain rate component in the slab ($\dot{\epsilon}_{SS}$) resolved parallel to the slab midplane. We show only the strong interior part of the slab: the subduction interface zone, upper plate, and parts of the mantle are above 1100°C isotherm have been masked. +ve values (blue) show zones of down-dip extension, -ve values (red) are shortening. Solid black lines show isotherms as labelled. Dashed black line is the slab midplane. Shaded green region represents the subduction interface. Inset in the panel at time 10 Myr shows the temperature and stress (horizontal component) profile in the plate at 300 km to the LHS of the trench. The upper panels show the curvature and curvature gradient of slab midplane, plotted along the same horizontal axes as the main panels (distance from trench).

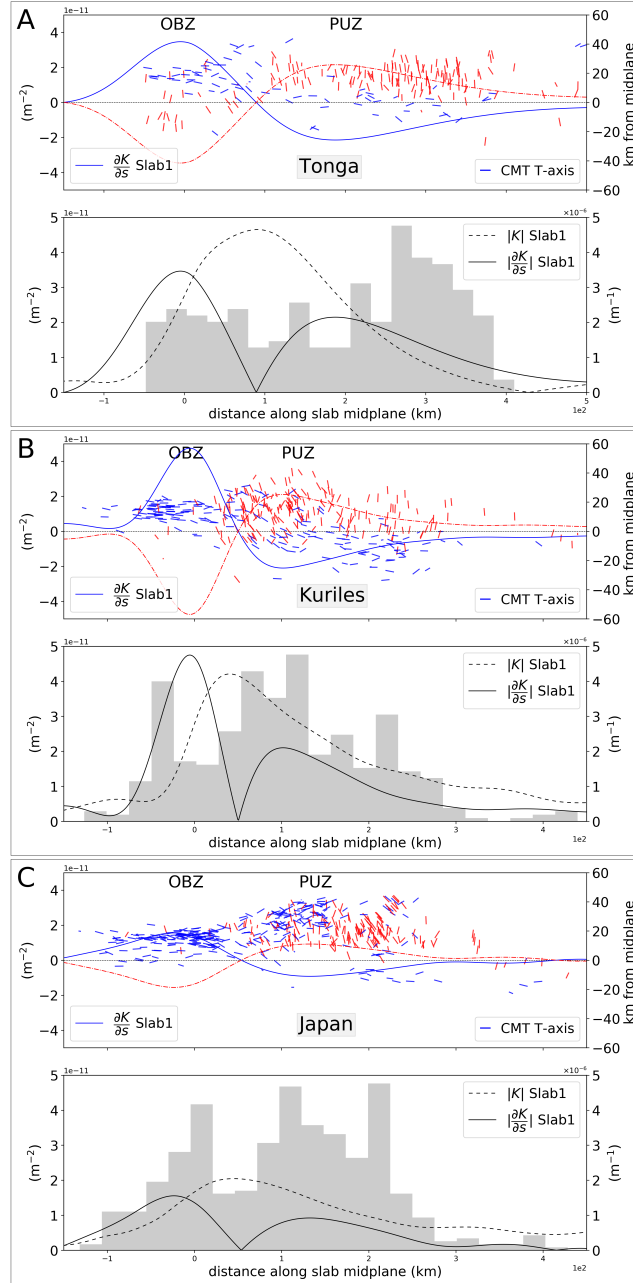


Figure 7: Summary of wPac slab seismicity-geometry relationships. a) Tonga, b) Kuriles, c) Japan. Top panels show CMT T-axes plotted in a slab midplane coordinate system, with distance from the hypocenter to the midplane on the vertical axis, and distance along the midplane relative to the trench on the horizontal axis. The T-axes have been rotated so that the angle relative to the midplane is preserved. The length variation in the plotted T-axes reflects the magnitude of the projected component of the vector. The blue solid line shows the value of the curvature gradient plotted against the distance along the midplane. The red dashed line shows the reflection of the curvature gradient about the midplane. Together, these lines show parts of the slab that are expected to be stretching (blue half) and shortening (red half), due to the geometric component of the bending rate. For each regions, the bottom panel includes a histogram showing the relative variation in number of slab earthquakes as a function of distance along the midplane with the solid and dashed lines showing the absolute value of the midplane curvature and the curvature gradient.

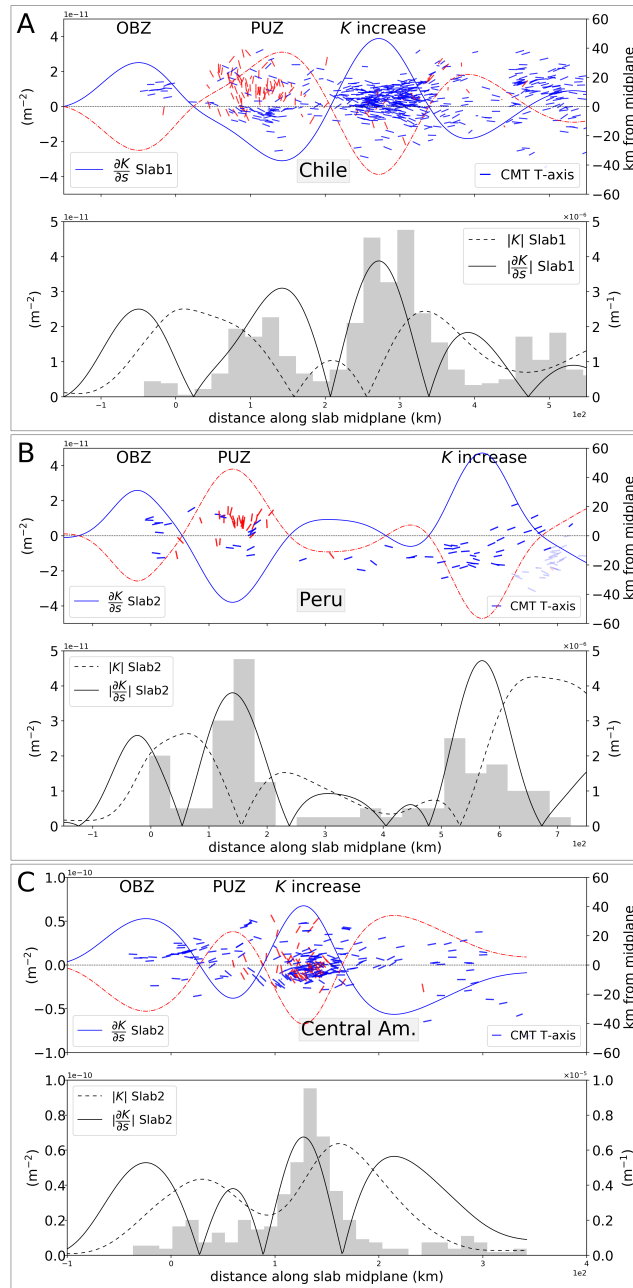


Figure 8: Summary of ePac slab seismicity-geometry relationships. a) Chile, b) Peru, c) Central America. See caption to Fig. 7 for further details.

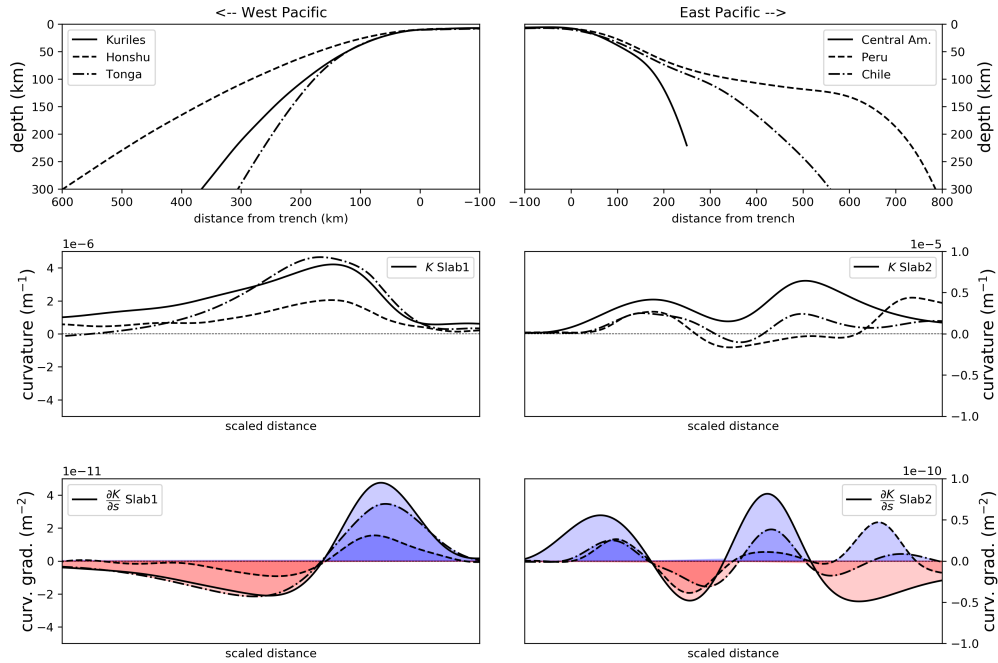


Figure 9: Comparison of characteristic features of wPac (left) and ePac (right) slab geometries. Upper panel shows slab profiles, middle panel shows curvatures and lower panels show curvature gradients. The geometric rate of bending is governed by the curvature gradient. In the lower two panels (either side) we have scaled the horizontal distance (distance along the midplane) so that the transition from the OBZ to the PUZ lies at the same point (i.e. the first zero crossing of the curvature gradient is equal for the ePac and wPac groups respectively). The color is indicative of the anticipated sense of deformation above the neutral plane: blue - extension, red - shortening.